DETERMINATION OF PROBABILITY OF FAILURE OF 20MnMoNi55 REACTOR PRESSURE VESSEL STEEL AT CRYOGENIC TEMPERATURES USING BEREMIN'S MODEL OF CLEAVAGE FRACTURE

A thesis submitted in partial fulfillment of the
requirement for the award of degree of

MASTER OF ENGINEERING

IN

CAD/CAM & ROBOTICS

By

MANJEET SINGH

(Student id - 80781014)

Under the guidance of

Dr. Rahul Chhibber
Lecturer
Mechanical Engineering Department,
Thapar University,
Patiala – 147004.

Dr. Bijan Kumar Dutta
Head
Computational Mechanics Section,
Reactor Safety Division,
Bhabha Atomic Research Center,
Mumbai – 400085.

Department of Mechanical Engineering

THAPAR UNIVERSITY ,

Patiala-147004 (INDIA)

July 2009

CERTIFICATE

This is to certify that The Thesis titled, **"DETERMINATION OF PROBABILITY OF FAILURE OF 20MnMoNi55 REACTOR PRESSURE VESSEL STEEL AT CRYOGENIC TEMPERATURES USING BEREMIN'S MODEL OF CLEAVAGE FRACTURE"** being submitted by **Mr. Manjeet Singh**, in partial fulfillment of the requirement for the award of **MASTER OF ENGINEERING (CAD/CAM & ROBOTICS) at THAPAR UNIVERSITY, PATIALA** is a bonafide work carried out by him under our guidance and no part of this thesis has been submitted for the award of any other degree.

Dr. Rahul Chhibber
Lecturer
Mechanical Engineering Department.
Thapar University,
Patiala - 147004

Dr. Bijan Kumar Dutta
Head
Computational Mechanics Section
Reactor Safety Division
Bhabha Atomic Research Center,
Mumbai - 400085

Dr. S.K. Mohapatra
Professor & Head
Mechanical Engineering Department
Thapar University,
Patiala - 147004

Dr. R.K. Sharma
Dean
Academic Affairs
Thapar University,
Patiala - 147004

ACKNOWLEDGEMENT

I would like to express a deep sense of gratitude and thanks profusely to my thesis guide **Dr. Rahul Chhibber,** (lecturer Department of Mechanical Engineering) Thapar University, PATIALA and **Dr. Bijan Kumar Dutta**, (Head Computational Mechanics section) Bhaba Atomic Research Centre, MUMBAI, for their Sincere and invaluable guidance, suggestion and sympathetic attitude which inspired me to submit this seminar report in the present form.

I am grateful to **Mr. Mahesh Sahu**, Scientific Officer (E), BARC. His suggestion and knowledge on the subject was invaluable throughout the thesis work.

I feel very much obliged to **Dr. S.K Mohapatra**, Professor & Head, Department of Mechanical Engineering and, Patiala for their intellectual support and **Dr. Abhijit Mukherjee**, Director, Thapar University, Patiala for giving us his precious time for teaching Computational Methods in CAD.

My special thanks are due to my **family** members who constantly encouraged me to complete this study and very special thanks to my elder brother **Karamjeet Singh Virk** for his assistance and guidance in code development.

Manjeet Singh

DATE: 15-07-09

Manjeet Singh

Student id - 80781014

ABSTRACT

The Nuclear Energy is of much importance in current scenario of World energy requirements, and also it is cleaner energy source than its current competitive mass Energy Production Techniques. Most of the nuclear energy being produced for peaceful purposes is obtained from nuclear plants which operate on Nuclear Fission process. Reactor Pressure Vessel (RPV) is an important part of such Nuclear Plants. In most Indian Nuclear Reactors the Steel used for fabrication of RPVs is German Steel designated as 20MnMoNi55, which is also used in current study. A large number of specimens are tested on various cryogenic temperatures to simulate the embrittlement caused by radiation from reactor and also embrittlement caused by Loss of Coolant Accident (LOCA). Under such circumstances it is important to know the cleavage fracture characteristics of the material, thus for this purpose the cleavage fracture behavior of material is predicted using Beremin's model of cleavage fracture, for this Weibull Stress (σ_u) and corresponding probabilities of failure (P_f) at different temperatures were determined in the current study.

TABLE OF CONTENTS

LIST OF FIGURES

LIST OF TABLES

CHAPTER - 1

INTRODUCTION

The energy consumption of world is increased in recent past, and will keep increasing due industrialization and increase in standard of living of human beings. In the next 50 years as earth's population expands from 6 billion to 9 billion, humanity will consume energy than the combined total used in all previous history.

Moreover, carbon emissions are now threatening the very stability of the earth, the well being of our humanity requires massive transformation to clean energy. The renewable energy like solar, wind and bio-mass can help but in limited capacity. Only nuclear power offers clean and environmentally friendly energy on mass scale. Fortunately, this urgently needed expansion can now build in half – century of tremendous advance in safe and secure operation of nuclear technology. A nuclear reactor produces and controls the release of energy from splitting the atoms of certain elements.

Reactor Pressure Vessel is very important part of nuclear reactors for the safe operation of Nuclear reactor. In Indian PHWR Nuclear reactors the Reactor Pressure Vessel Steel used is 20MnMoNi55. RPV is prone to direct radiations from the reactor core which cause embrittlement of RPV material in long run, also In case of Loss of Coolant Accident (LOCA) in which reactor core is flooded with coolant lowering the temperature of the reactor and RPV which causes increase in the Ductile to Brittle Transition Temperature (DBTT) thus embrittlement of the RPV. Thus for the safe operation of reactor it's necessary to know the Cleavage Fracture characteristics of RPV steels. A brief introduction of Nuclear reactor components and Reactor Pressure Vessel is as follows:

1.1 Nuclear Reactor

There are several components common to most types of Nuclear reactors:-

1. Fuel - Usually pellets of uranium oxide (UO_2) arranged in tubes to form fuel rods. The rods are arranged into fuel assemblies in the reactor core.

2. Moderator - This is material which slows down the neutrons released from fission so that they cause more fission. It is usually water, but may be heavy water or graphite.

3. Control rods - These are made with neutron-absorbing material such as cadmium or boron, and are inserted or withdrawn from the core to control the rate of reaction, or to halt it.

4. Coolant - A liquid or gas circulating through the core so as to transfer the heat from it. . In light water reactors the water moderator functions also as primary coolant.

5. Pressure vessel or pressure tubes - Usually a robust steel vessel containing the reactor core and moderator/coolant, but it may be a series of tubes holding the fuel and conveying the coolant through the moderator.

6. Steam generator - Part of the cooling system where the heat from the reactor is used to make steam for the turbine.

7. Containment - The structure around the reactor core which is designed to protect it from outside intrusion and to protect those outside from the effects of radiation in case of any malfunction inside. It is typically a metre-thick concrete and steel structure.

1.2 Reactor Pressure Vessel

A typical RPV is shown in Figure 1.1. The RPV is cylindrical with a hemispherical bottom head and a flanged and gasketed upper head. The bottom head is welded to the cylindrical shell while the top head is bolted to the cylindrical shell via the flanges. The cylindrical shell course may or may not utilize longitudinal weld seams in addition to the girth (circumferential) weld seams. The body of the

vessel is of low-alloy carbon steel. To minimize corrosion, the inside surfaces in contact with the coolant are clad with a minimum of some 3 to 10 mm of austenitic stainless steel. Numerous inlet and outlet nozzles, as well as control rod drive tubes and instrumentation and safety injection nozzles penetrate the cylindrical shell. The number of inlet and outlet nozzles is a function of the number of loops or steam generators.

1.3 Fabrication of RPVs

Fabrication of RPVs has also been an evolving technology, and later vessels were fabricated using knowledge gained from the surveillance programs and more modern methods such as the use of large forgings to reduce the number of welds in the beltline

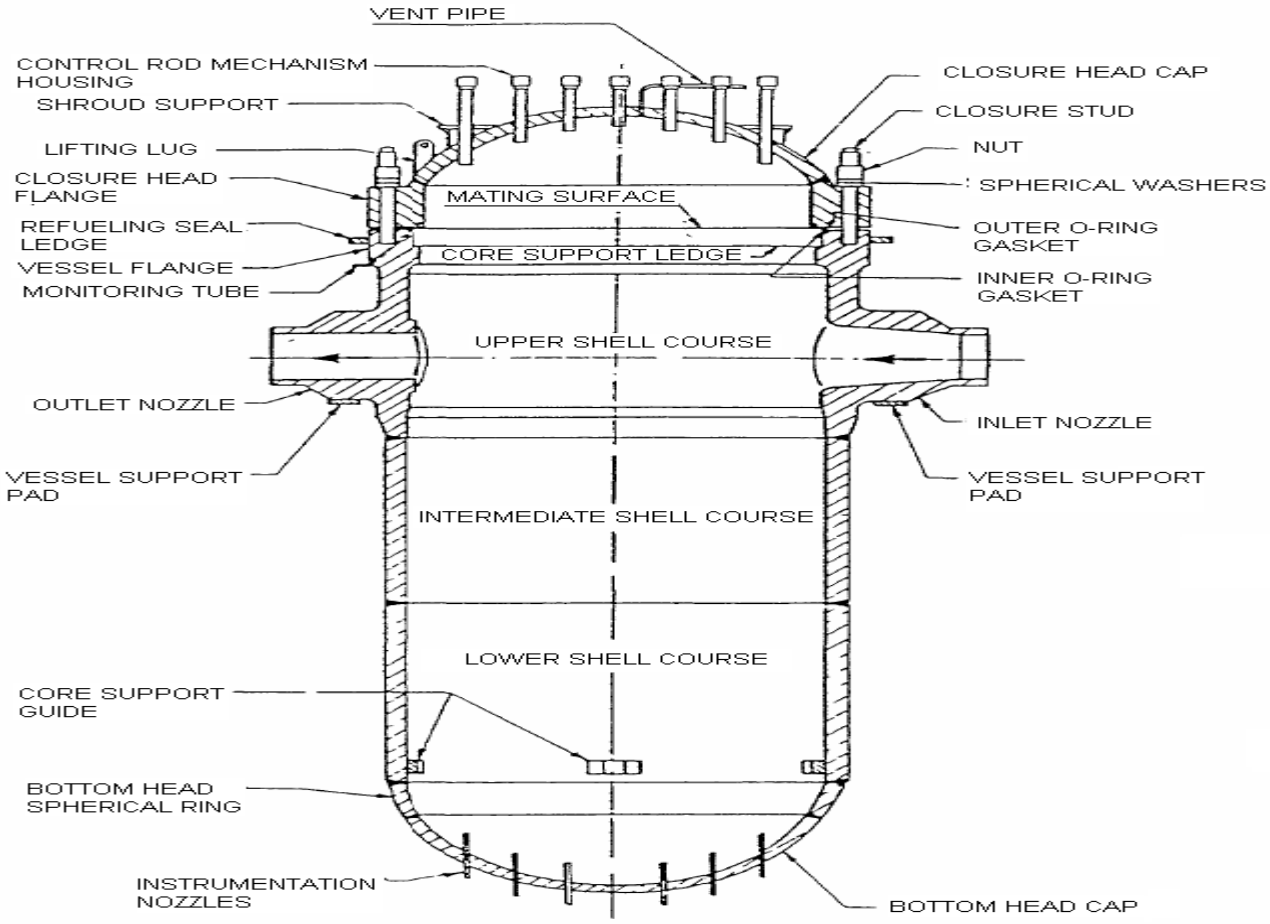

Figure 1 - 1 A Typical Nuclear Reactor Pressure Vessel

Large vessels are generally fabricated by two methods. In the first method, rolled and welded plates are used to form separate steel courses. Such a vessel has both longitudinal and circumferential weld seams (Figure 1.8a). In the second method,

large ring forgings are used (Figure 1.8b). This method improves component reliability because of the lack of longitudinal welds. Weld seams are located to avoid intersection with nozzle penetration weldments. Weldments within the beltline region were minimized once research showed that weld metal could be more sensitive to neutron radiation than base material. In general, parts of the longitudinal shell course welds are within the beltline region when the RPV is fabricated using plate material.

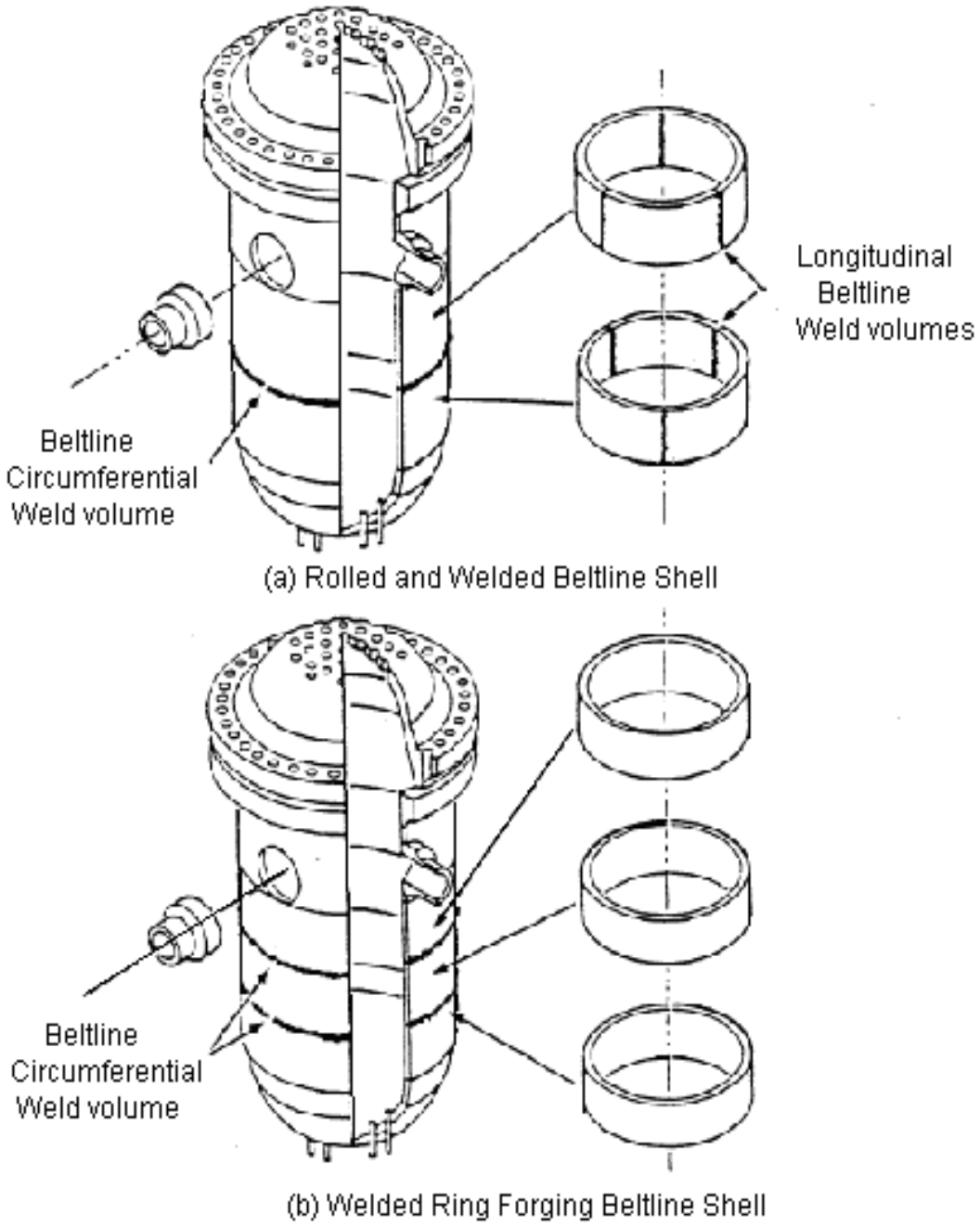

Figure 1 - 2 Fabrication configurations of PWR beltline shells

1.4 Reactor Pressure Vessel Material

In RPVs different materials are used for the different components (shells, nozzles, flanges, studs, etc.). Moreover, the choices in the materials of construction changed as the PWR products evolved. For example, the Westinghouse designers specified American Society for Testing and Materials (ASTM) SA 302 Grade the shell plates of earlier vessels and ASTM SA 53 Grade B Class 1 for later vessels. Other vessel materials in common use include American Society of Mechanical Engineers (ASME) SA 508 Class 2 plate in the USA, 22NiMoCr37 and 20MnMoNi55 in Germany, and 16MnD5 in France. SA-302, Grade B is a manganese-molybdenum plate steel used for a number of vessels made through the mid-1960s. Its German designation is 20MnMo55. As commercial nuclear power evolved, the sizes of the vessels increased. For the greater wall thicknesses required, a material with greater hardening properties was necessary. The addition of nickel to SA-302, Grade B in amounts between 0.4 and 0.7 weight per cent provided the necessary increased hardening properties to achieve the desired yield strength and high fracture toughness across the entire wall thickness. This steel was initially known as SA-302, Grade B Ni Modified.

Forging steels have also evolved since the mid-1950s. The SA-182 F1 Modified material is a manganese-molybdenum-nickel steel used mostly for flanges and nozzles in the 1950s and 1960s. Another forging material used then was a carbon-manganese-molybdenum steel, SA- 336 Fl. Large forgings of these materials had to undergo a cumbersome, expensive heat treatment to reduce hydrogen blistering. Eventually these steels were replaced with steel, first described as ASTM A366 Code Case 1236 and are now known as SA-508 Class 2, that did not require this heat treatment. This steel has been widely used in ring forgings, flanges and nozzles. It was introduced into Germany with the designation 22NiMoCr36 or 22NiMoCr37. With slight modifications, this steel became the most important material for German reactors for a long time. In addition, SA-508 Class 3 (20MnMoNi55 in Germany and 16 MnD5 and 18MnD5 in France) is used in the fabrication of RPVs.

CHAPTER - 2

LITERATURE REVIEW

2.1 Irradiation Effects

It is well known that bombardment of metals by energetic neutrons induces considerable changes in their physical and mechanical properties. An increase in yield stress associated with a reduction in ductility was observed in RPV steels used for cladding of RPV. Also Reduction in Corrosion resistant properties was observed. [14]

Metallographic studies showed considerable differences in microstructure of the steel in unirradiated and irradiated states [16]. The relative proportions of the sorbite and ferrite grains in the unirradiated steel and irradiated steel shows considerable variation as apparent from Figure 2.1. It should also be noted that in the unirradiated steel the sorbite grains are very distinct, i.e., the grain boundaries are very clearly defined and always continuous in nature. After irradiation, the boundaries are less distinct, becoming smaller, with their grain boundaries broken and unfinished. The discovery shows that many of the “secondary” ferrite grains, i.e., grains that formed as a result of the simultaneous effect of radiation, temperature, and stress, were extended (in some cases in twin formation) along certain directions in a specimen. When viewed on the macroscale, these grains appear to be organized and one can discern certain recurring patterns.

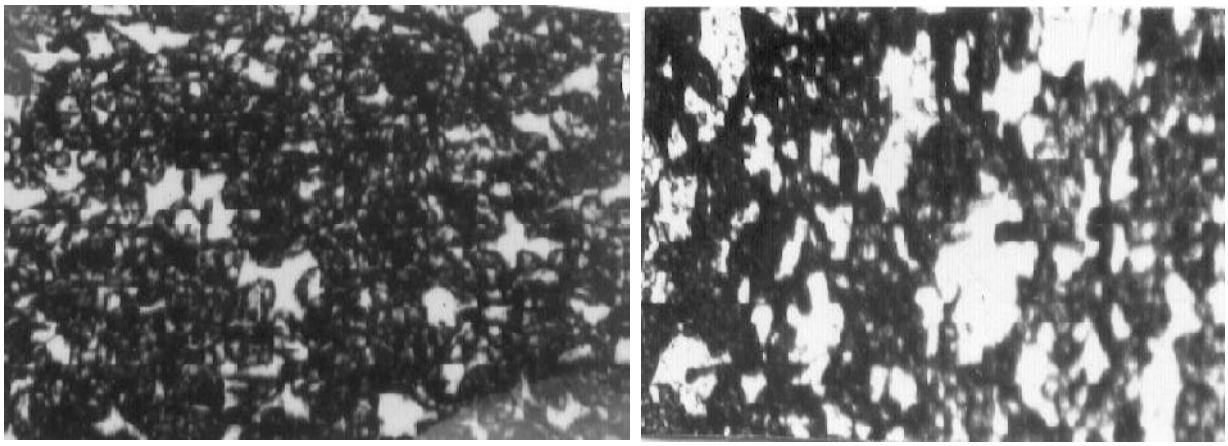

(a) irradiated EP-450 steel (x 200) .[16] **(b) Unirradiated EP-450 steel (x 200) [16].**

Figure 2 - 1 Microstructure of Steel Dark areas are sorbite grains; light areas are ferrite grains

Eighty percent of the energy released by the Deuterium - Tritium fusion reaction is transferred by 14 MeV neutrons to the first wall and breeding blanket. The remaining 20% are carried by α-particles issued from the same reaction that together with other low energy neutral and charged particles will induce sputtering, erosion and blistering in the plasma facing materials. About 10% of the energy of the 14 MeV neutrons will be deposited in the first wall, the remaining energy being transferred mostly to the blanket [17]

2.1.1 Microscopic Causes of RPV Embrittlement

The microscopic causes of embrittlement lie in the forming of obstacles to dislocation motion, called “hardening centers”, as well as to changes of the composition and structure of the microscopic interfacial regions along which crystal plane sliding occurs. Both these phenomena are caused by several types of radiation-matter interactions, most of which are, in LWRs, induced by fast neutrons. Also γ-rays, in less frequent circumstances, may give a substantial contribution. From this consideration it follows that fast neutron irradiation is not the only cause of vessel wall embrittlement, even though its contribution is very often the dominant one [15].

The following subsections describe briefly the mechanisms causing embrittlement [15].

2.1.1.1 Neutron Irradiation

Neutrons cause embrittlement mainly through two mechanisms: Atom Displacement and Induced Helium Production Reaction.

The microscopic structural damage resulting from the collision between an incoming neutron and a stationary nucleus is more extensive when the incoming particle is highly energetic, i.e. when the neutron is a fast neutron. However, an accurate prediction of the radiation damage cannot account only for the consequences of the occurrence of a postulated collision event, but also for the probability that this event can actually occur. In this regards, thermal neutrons turn out to have a moderately high displacement cross section

Since boron is often present in RPV steels as impurity, neutron irradiation can yield helium production. Then, the bubbles so formed tend to coalesce at the grain

boundaries, initiating the so-called grain-boundary cracking, which causes structure embrittlement.

2.1.1.2 Gamma-Ray Irradiation

There are Several reactions that give origin to γ-rays. A strong source is the fissioning fuel in the reactor core, but also the peripheral structure materials can interact with thermal and fast neutrons and undergo reactions in which such radiations are emitted. Then, they may cause atom displacements in the vessel wall material by transferring their energy to electrons via Compton scattering, pair production and photoelectric effect.

Embrittlement: macroscopic effects, indicator parameters and quantitative prediction macroscopic effects of embrittlement

As mentioned before, embrittlement is the reduction of toughness of a material, which is in turn the maximum energy that the material can absorb before rupturing and secondary consequence of irradiation, i.e. the increase of yield and ultimate strength.

2.2 Ductile-Brittle Transition Temperature

The ductile-brittle transition temperature (DBTT), nil ductility temperature (NDT), or nil ductility transition temperature of a metal represents the point at which the fracture energy passes below a pre-determined point (for steels typically 40 J [13] for a standard Charpy impact test). DBTT is important since, once a material is cooled below the DBTT, it has a much greater tendency to shatter on impact instead of bending or deforming. For example, zamak 3 exhibits good ductility at room temperature but shatters at sub-zero temperatures when impacted. DBTT is a very important consideration in materials selection when the material in question is subject to mechanical stresses.

In some materials this transition is sharper than others. For example, the transition is generally sharper in materials with a body-centered cubic (BCC) lattice than those with a face-centered cubic (FCC) lattice. DBTT can also be influenced by external factors such as neutron radiation, which leads to an increase in internal lattice defects and a corresponding decrease in ductility and increase in DBTT.

According to USNRC Regulatory Guide 1.99 Rev. 2, the shift in DBTT (in 0F) as a function of the neutron fluence is given by:

$$\Delta DBTT = [CF] \times f\,(0.28 - 0.1 \log f)$$

Where CF is a function of the weight percentages of copper and nickel in the material. Here, f is the fluence in the unit of 1019 n/cm^2.

2.3 Fracture Mechanics

Fracture mechanics is the field of solid mechanics that deals with the behavior of cracked bodies subjected to stresses and strains. These can arise from primary applied loads or secondary self-equilibrating stress fields (e.g. residual stresses).

Fracture (definition) - "It is defined as separation or fragmentation of body into two or more parts under the action of stress. The process of fracture can be considered to be made up of two components i.e. crack initiation and crack propagation. Fractures can occur under all service conditions. Material subjected to cyclic loading fail due to fatigue and material used at high temperature can fail due to creep rupture."

The fracture of any material occurs in two steps:

1. Crack formation
2. Crack Propagation

The failure of engineering materials is classified in terms of being:

1. Ductile: significant plastic deformation prior to fracture
2. Brittle: little or no plastic deformation prior to fracture

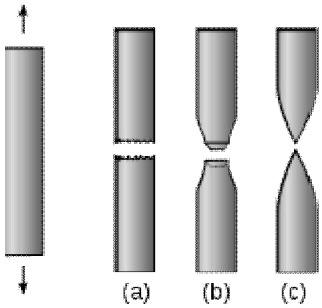

Figure 2 - 2 Schematic Appearance of Round Metal Bars After Tensile Testing

(a) Brittle fracture; (b) Ductile fracture; (c) Completely ductile fracture

From investigating fallen structures, engineers found that most failure began with cracks. These cracks may be caused by material defects (dislocation, impurities...), discontinuities in assembly and/or design (sharp corners, grooves, nicks, voids...), harsh environments (thermal stress, corrosion...) and damages in service (impact, fatigue, unexpected loads...). Most microscopic cracks are arrested inside the material but it takes one run-away crack to destroy the whole structure.

To analyze the relationship among stresses, cracks, and fracture toughness, Fracture Mechanics was introduced. The first milestone was set by Griffith in his famous 1920 paper that quantitatively relates the flaw size to the fracture stresses. However, Griffith's approach is too primitive for engineering applications and is only good for brittle materials.

For ductile materials, the milestone did not come about until Irwin developed the concept of strain energy release rate G in 1950s.When the strain energy release rate reaches the critical value, the crack will grow. Later, the strain energy release rate was replaced by the stress intensity factor K with a similar approach by other researchers. After the fundamentals of fracture mechanics were established around 1960, scientists began to concentrate on the plasticity of the crack tips. In 1968, Rice modeled the plastic deformation as nonlinear elastic behavior and extended the method of energy release rate to nonlinear materials. He showed that the energy release rate can be expressed as a path-independent line integral, called the J-integral. Rice's theory has since dominated the development of fracture mechanics in Unite States. Meanwhile, Wells proposed a parameter called crack tip opening displacement (CTOD), which led the fracture mechanics research in Europe. Thereafter, many experiments were conducted to verify the accuracy of the models of fracture mechanics.

Significant efforts were devoted to converting theories of fracture mechanics to fracture design guidelines. Recent trends of fracture research include dynamic and time-dependent fracture on nonlinear materials, fracture mechanics of microstructures, and models related to local, global, and geometry- dependent fractures.

2.3.1 Classification of Fracture Mechanics

Two Important Classifications of Fracture mechanics are:

1. Linear Elastic Fracture Mechanics (LEFM) e.g. Glass.
2. Elastic Plastic Fracture Mechanics (EPFM) e.g. Mild steel.

In the regime where the global stress-strain response of the body is linear and elastic (LEFM), the stress intensity factor K is used. In the plastic collapse region, design can be done on the basis of ensuring that net section yield does not occur, whilst in the elastic-plastic region EPFM, nowadays called yielding fracture mechanics YFM, is applicable. The fracture characterizing parameters in YFM are the J-integral and the crack opening displacement, COD. All these fracture characterizing parameters meet both the Griffith energy criterion for fast crack growth, and the critical stress/strain criterion. For simple cases, fracture problems can be approached via the Griffith equation, which is particularly suitable for sharp cracks/defects in brittle materials.

2.3.1.1 Linear Fracture Mechanics (LEFM)

Linear Elastic Fracture Mechanics (LEFM) first assumes that the material is isotropic and linear elastic. Based on the assumption, the stress field near the crack tip is calculated using the theory of elasticity. When the stresses near the crack tip exceed the material fracture toughness, the crack will grow. In Linear Elastic Fracture Mechanics, most formulas are derived for either plane stresses or plane strains, associated with the three basic modes of loadings on a cracked body: opening, sliding, and tearing. Again, LEFM is valid only when the inelastic deformation is small compared to the size of the crack, what we called small-scale yielding. If large zones of plastic deformation develop before the crack grows, Elastic Plastic Fracture Mechanics (EPFM) must be used.

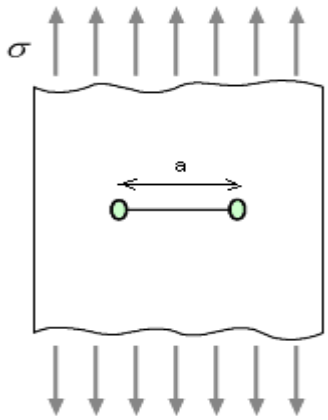

Figure 2 - 3 Linear Elastic Crack In Tensile Specimen

Most metallic alloys and thermo set polymers are considered isotropic, where by definition the material properties are independent of direction. Such materials have only two independent variables (i.e. elastic constants) in their stiffness and compliance matrices. The two elastic constants are usually expressed as the Young's modulus E and the Poisson's ratio □. However, the alternative elastic constants K (bulk modulus) and/or G (shear modulus) can also be used. For isotropic materials, G and K can be found from E and □ by a set of equations, and vice-versa

2.3.1.2 Elastic Plastic Fracture Mechanics (EPFM)

Linear Elastic Fracture Mechanics (LEFM) applies when the nonlinear deformation of the material is confined to a small region near the crack tip. For brittle materials, it accurately establishes the criteria for catastrophic failure. However, severe limitations arise when large regions of the material are subject to plastic deformation before a crack propagates. Elastic Plastic Fracture Mechanics (EPFM) is proposed to analyze the relatively large plastic zones.

Elastic Plastic Fracture Mechanics (EPFM) assumes isotropic and elastic-plastic materials. Based on the assumption, the strain energy fields or opening displacement near the crack tips are calculated. When the energy or opening exceeds the critical value, the crack will grow.

Although the term elastic-plastic is used in this approach, the material is merely nonlinear-elastic. In others words, the unloading curve of the so called elastic-plastic

material in EPFM follows the original loading curve, instead of a parallel line to the linear loading part which is normally the case for true elastic-plastic materials.

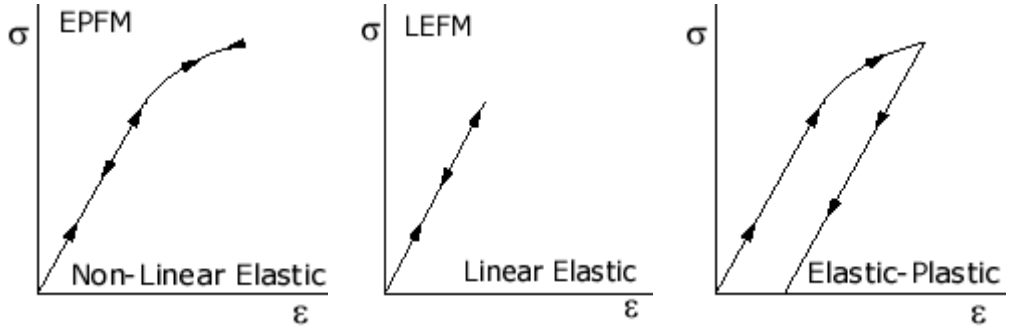

Figure 2 - 4 Difference between LEFM, EPFM

2.4 Micromechanical Modeling / Damage Mechanics

The fundamental difference between fracture mechanics and damage mechanics is that in damage mechanics we consider the void, nucleation and coalescence while in fracture mechanics we do not consider any voids formation in metal matrix. The distance between the nucleuses of two voids is of micro level that's why it comes under micro mechanical Modeling.

The mechanism of cleavage fracture in reactor pressure retaining material is significantly different from ductile fracture. The cleavage fracture in a material usually originates from micro-cracks, which are formed by different mechanisms. The micro-cracks are formed due to a non-homogeneous distribution of plastic deformation within the grains, called slip-initiated cleavage. The cracked grain boundary carbides also are the sources to originate the micro-cracks. This occurs when the stress normal to the planes of carbide particles is sufficiently high. The fracture takes place by the formation of micro-cracks and their extension with little global plastic deformation. The cleavage process is stress controlled and consumes little deformation energy and hence, the crack grows unstably fast. In this case the local fracture criterion is generally based on a critical cleavage stress.

Based on weakest link assumption [1] and Weibull statistics, Beremin developed a model for the analysis of cleavage fracture process [2]. Present work is based on two-parameter Weibull statistics. These parameters, termed Beremin's parameters, are determined using experimental fracture data and finite element (FE) analysis and are essential to predict probability of cleavage fracture in a component. Experimental data includes the load and deformation at failure whereas FE analysis gives the stress distribution in the test specimen at failure.

2.4.1 Beremin's Model For Cleavage Fracture

The Cleavage fracture in a material usually originates from microcracks which are formed by different mechanisms. The microcracks are formed due to an inhomogeneous distribution of plastic deformation within the grains. It is called slip initiated cleavage. In mild steels the cracked grain boundary carbides also originates the microcracks. This occurs when the stress normal to the planes of carbide particles is sufficiently high. This critical stress, σ_c, required for the separation of cleavage facets, can be related to the length 'l_0' of a microcrack by the equation

$$\sigma_c = \sqrt{\frac{2E\gamma}{\pi(1-v^2)l_0}} \qquad \textbf{1 - 1}$$

Where E is Young's modulus of elasticity, v is Poisson's ratio, and γ is the surface energy. The length 'l_0' is related to the dimensions of the relevant metallurgical features associated with stable microcracks. In mild steel, the grain boundary carbide width is considered as the relevant metallurgical length. The probability of finding a microcrack of critical length is a function of the volume of the material involved. It is very difficult to find out this probability experimentally. In a population of microcracks, the fracture will take place at the site of longest microcrack. Therefore the knowledge of distribution of microcracks is required for the longer ones. Let us assume that the stressed volume can be divided in smaller volumes V_0. This V_0 should be large enough to the extent that the probability of finding a microcrack of reasonable length is not very small and the statistical independence of neighboring volumes can be assumed. In each volume, the probability of finding a crack of length between l_0 and $l_0 + dl_0$ can be written as:

$$P(l_0)dl_0 = \frac{\alpha}{l_0^{\beta}} dl_0 \qquad \textbf{1 - 2}$$

Where α and β are material constants for a particular value of V0. Hence in a given volume where the stress level is σ, the probability of failure is:

$$P(\sigma) = \int_{l_0^c}^{\infty} P(l_0)dl_0 = \left[\frac{\alpha}{(1-\beta)} \cdot \frac{l}{l^{\beta-1}_{0}}\right]_{l_0^c}^{\infty} = \frac{\alpha}{(\beta-1)} \cdot \frac{l}{l_0^{c(\beta-1)}} \qquad \textbf{1 - 3}$$

Where l_0^c is given by equation [1] as:

$$l_0^c = \frac{2E\gamma}{\pi(1-v^2)\sigma^2} \qquad \textbf{1 - 4}$$

Putting equation (4) in equation (3), we get:

$$P(\sigma) = \left(\frac{\sigma}{\sigma_u}\right) \qquad \textbf{1 - 5}$$

Where m= 2β-2 and $\sigma_u^m = \frac{(\beta-1)(2E\gamma)^{(\beta-1)}}{\alpha.\pi^{\beta-1}.\ (1-v^2)^{\beta-1}} .\sigma_u$ turns out to be a material constant almost independent of temperature if it is assumed that γ does not change with temperature. The stressed region of the specimen is divided into n volumes of V_0. Each volume, number i, subjected to a quasi-homogeneous stress state σ_i, where σ_i is the maximum principal stress. This implies that the stress variation in V_0 is chosen small enough. For the notched tensile specimens, the failure probability of the volume number 'i' will be $P(\sigma_i)=(\sigma_i/\sigma_u)^m$. The cumulative probability of failure for the entire specimen (i.e. for volume number i=1, n) is given by:

$$P_R = 1 - \prod_{i=1}^{n}[1 - P(\sigma_i)] \qquad \textbf{1 - 6}$$

Since P(σi) is small, it can be written as:

$$\ln(1 - P_R) = \sum_{i=1}^{n} \ln[1 - P(\sigma_i)] \approx \sum_{i=1}^{n} -P(\sigma_i) \qquad \textbf{1 - 7}$$

2.4.1.1 Failure Probability For Homogeneously Stressed Specimens:-

Assuming a constant stress σ over the whole volume (i.e. for a homogeneously stressed specimen), this expression can be written as:

$$\ln(1 - P_R) = -\frac{V}{V_0}\left(\frac{\sigma}{\sigma_u}\right)^m \qquad \textbf{1 - 8}$$

Which is one form of the Weibull expression. The average stress at rupture is given by:

$$(\sigma_R) = \sigma_u \left(\frac{V_0}{V}\right)^{1/m} \left(\frac{1}{m}\right)! \qquad \textbf{1 - 9}$$

It is worth emphasizing that two parameters are required for the definition of the probability of failure of the entire specimen, i.e. m and $\sigma_u^m V_0$. However, V_0 must be of the order of ten grains, i.e. small enough to neglect stress gradients in $V_0$and large enough to assume statistical independence of individual volumes V_0. If very small gradients are present in the specimen, then V_0 can be arbitrarily chosen.

Usually V_0 is chosen as a cubic volume containing about 8 grains of the material, i.e.50x50x50 μm. These small dimensions are adopted in relation to the mesh size used in finite element calculations

2.4.2.2 Failure Probability For Non-Homogeneously Stressed Specimens:-

For non-homogeneously stressed specimens, the equation (7) is used for calculating failure probability. Putting equation (5) in equation (7), we get:

$$\ln(1 - P_R) = \sum_{i=1}^{n} -P(\sigma_i) = -\sum_{i=1}^{n}\left(\frac{\sigma_1^i}{\sigma_u}\right)^m \frac{V_i}{V_0} = \left[-\left(\frac{\sigma_w}{\sigma_u}\right)^m\right] \qquad \textbf{1 - 10}$$

$$\Rightarrow P_R = 1 - \exp\left[-\left(\frac{\sigma_w}{\sigma_u}\right)^m\right] \qquad \textbf{1 - 11}$$

Where V_i is the volume of the ith element experiencing the maximum stress σ_1^i and σ_w is called the "Weibull Stress" and is defined as:

$$\sigma_w = \sqrt[m]{\sum_{i=1}^{n} (\sigma_1^i)^m \frac{V_i}{V_o}} \qquad \textbf{1 - 12}$$

2.5 Work Reviewed

Earlier experiments performed several centuries' ago by Leonardo de Vinci provided some clues as to the root cause of fracture. He measured the strength of iron wires and found that the strength varied inversely with wire length. These results implied that flaws in material controlled the strength; a longer wire corresponded to a larger sample volume and a higher probability of sampling a region containing flaw. These results were qualitative in nature.

A quantitative connection between fracture stress and flaw size came from the work of Griffith [3], which was published in 1920. He applied a stress analysis of an elliptical hole to the unstable propagation of a crack. Griffith invoked the first law of thermodynamics to formulate a fracture theory based on a simple energy balance. Griffith's model correctly predicted the relationship between strength and flaw size in glass specimens. Subsequent efforts to apply Griffith model to metals were unsuccessful. Since this model assumes the work of fracture exclusively comes from the surface energy of material, the Griffith approach only applies only to ideally brittle solids.

Then came the famous liberty ship incident during World War II. These ships were completely welded. There was large number of failures of these ships. Some of the ships broke into two parts. Investigation revealed the ship failures were combination of three factors: weld defects, stress concentration at some locations and poor material used. Once the reasons of failure were identified, Corrective actions were

taken whine manufacturing these Liberty ships in future. However, it led to a more detailed fracture research program in US Naval Research Laboratory in Washington DC under the leadership of Dr. G.R. Irwin. The first major contribution of Irwin was to modify the Griffiths approach to metals by including the energy dissipated by local plastic flow. In 1956, Irwin [4] developed energy release rate concept, which is related to Griffith theory, but in a form, which is more useful to solve engineering problems. Afterwards, Irwin developed the equation of the stress and strain field around a crack in an infinite plate using the Westergaard stress function approach. This paved the way for the development of a new field, known as Fracture Mechanics. A number of successful applications of fracture mechanics bolstered the standing of this new field in the engineering community.

The original motivation for development of fracture mechanics was to be able to account for materials that fracture with limited plastic deformation- that is, at applied stress levels less than those producing net section yielding. The discipline was initially focused on linear elastic brittle behavior. But, with the successes that were achieved with LEFM, materials for which such an approximation would be invalid also became of interest. To address the integrity of components made of these type of ductile materials in the presence of crack like defects, an alternative fracture mechanics model named as 'Elastic Plastic Fracture Mechanics' (EPFM) developed in late sixties and at later decades. Major thrust in the development of EPFM came in the late seventies and eighties when it was being extensively used to assess the integrity of piping of various nuclear power plants all over the world.

B. K. Dutta, et al. [5] - The temperature dependency of Beremin's parameters has been investigated for 20MnMoNi55 material. Tensile tests have been conducted on specimens having central groove at subzero temperatures.. The analytical study has been carried out to determine Beremin's parameters using the statistical variation in load v/s diametrical contraction. For this purpose, finite element analyses have been carried out for each specimen to determine Weibull stress during fracture. The experimental probability of failure of each specimen has been calculated by ranking them based on the load as well as diametrical contraction at the time of fracture. Such a table along with the Weibull stresses are used in the equations derived using "maximum likelihood method" to derive the Beremin's parameters.

Cleizergues et al. [6] - This paper describes the use of Local Approach to Fracture in the French steel industry. The criteria used to model cleavage fracture of steels are briefly presented. Various applications covering a wide range of steels are reviewed. These applications illustrate the advantages of the Local Approach, such as scatter prediction, the ability to finely relate microstructure to mechanical properties and to take into account materials with heterogeneous microstructures such as welds. Finally, current developments of the method are presented. These developments will allow a quick and easy implementation of this procedure which will become accessible to industrial laboratories

GY. B. LENKEY, et al. [7] – The Beremin model of brittle fracture was implemented for cast ferritic steel materials using In House finite element code. The effect of different material parameters (like yield stress, strain hardening exponent) was investigated on the Beremin model's parameters. Also it was analyzed how the applied numerical procedure affects these results. As it was found, the strain hardening exponent has small effect on the model parameters, the yield stress has stronger effect. The applied fitting method can cause larger differences. The numerical values of the Weibull-parameters depend strongly on the scatter of the measured fracture probability values. Then the fracture behavior of Charpy-V specimens was predicted by applying the obtained Beremin-model's parameters. The accuracy of the prediction mostly depends on the variation of the yield stress.

A Mirzaee-Sisan, et al. [8]- In this paper application of the local approach to predict the fracture behavior of A533B ferritic steel at low temperature, in presence of a residual stress field, is investigated. The local approach assumes a Weibull probability distribution for the fracture toughness data and is based on the work of the Beremin model. In the work presented here, the Weibull parameters are calibrated to fracture data obtained at low temperature for specimens containing no residual stress fields. The same parameters are then used to predict the fracture behavior of specimens containing a residual stress field which has been introduced by the local compression technique. Local approach predictions obtained using finite element analysis and experiments demonstrated a reduction in the low temperature

fracture toughness of laboratory specimens following local compression. However, the decrease in experimental fracture toughness data is not as high as predicted by numerical simulations using the local approach.

D. Moinereau, et al. [9] – This was a Cooperative research programme in the field of the local approach to cleavage fracture applied to reactor pressure vessels is conducted between EDF, CEA, Framatome and AEA Technology. The purpose of the programme was to have better knowledge of this approach for RPV fracture mechanics integrity assessments regarding the risk of brittle fracture. This programme included both an experimental part conducted by several laboratories in order to identify m and σ_u parameters of Beremin model on a A508 C13 steel, and numerous numerical computations of specimens and structures. Finite element programs are compared on some reference calculations in order to validate local approach to fracture postprocessors. The capability of Beremin model to explain the shallow flaw effect in cleavage fracture is finally discussed.

Gy. B. Lenkey, et al.[10] - The aim of our work was to study the applicability of the Beremin-model for predicting the brittle fracture behavior of ferritic cast steel used for spent nuclear fuel containers, and to study the sensitivity of the model for different material parameters. The model parameters were determined according the recommended ESIS procedure on the basis of experiments on notched tensile specimens performed at -160. The fracture loads and fracture probabilities of V-notched Charpy-type specimens were determined and compared with experimental data.

Takashi Miyata, et al. [11] - The cleavage fracture toughness of steels was mezzo-scopically analyzed on the basis of the statistical local fracture criterion approach. The statistical stress criterion at the crack tip region suggests that the cleavage fracture toughness in steels can be described as a function of the yield stress, the cleavage fracture stress, and other mechanical properties of the materials. Formulation of the cleavage fracture toughness was first examined through an investigation on correlation between the cleavage toughness and the cleavage

fracture stress obtained in notched round bar specimens in accordance with the theoretical prediction.

C. Ruggieri [12] This study extends the Weibull stress approach to address effects of strength mismatch on macroscopic fracture toughness of interface cracks. The approach builds on the Beremin model to establish a relationship between the micro regime of fracture and macroscopic crack driving forces for bi-material media by adopting the Weibull stress (σ_w) as a probabilistic fracture parameter. Plane-strain, small scale yielding (SSY) reference fields for stationary interface cracks are presented to provide a measure of mismatch effects. The analyses show a strong effect of mismatch level on the magnitude of the Weibull stress which enables assessments of fracture behavior in interface cracks.

CHAPTER - 3

PROBLEM DEFINITION

3.1 Introduction

Components like reactor pressure vessel (RPV) which use ferritic steel operate under high neutron flux over considerably long period of time. Hence, it is essential to access the structural integrity of the vessel under accidental scenario. This kind of analysis finds more relevance at higher fluenece levels, i.e. when the vessel becomes more aged. The analysis scenario considers the occurrence of 'loss of coolant accident' (LOCA) and subsequently the reactor core gets flooded through emergency core cooling system. The cooling of the vessel material can bring down the temperature to ductile brittle region. Under such conditions the microcracks in the component subjected to tensile stresses may lead to unstable cleavage fracture. Information on such fracture behavior of the material at transition region is mandatory to quantify the inherent safety margin available under such undesirable events.

3.2 Aim of Thesis

Different materials used for RPVs are described in section 1.4, although many materials are acceptable for reactor pressure vessels, the special considerations pertaining to fracture toughness and radiation effects effectively limit the basic materials acceptable for most parts of reactor pressure vessels.

Cleavage fracture in ferritic steels usually occurs by unstable micro-cracks initiated at brittle second phase inclusions. Due to the scatter in such factors such as size, orientation and shape of such inclusions, and the non uniform stress field around a loaded crack tip, the event of cleavage fracture has statistical nature. To predict the cleavage fracture initiation, the Beremin's model of cleavage fracture based on weakest link theory and incorporating two parameter Weibull statistics is used is used in the study. The aim of this work is to determine the critical Weibull parameter of the model from the experimental results from a number of specimens tested at cryogenic temperatures. The maximum likelihood method is used to determine the parameters. The material studied was German steel 20MnMoNi55. The parameters were determined by ranking the specimens according to the load at fracture of the specimen during experimentation.

CHAPTER - 4

Experimentation and Finite Element Analysis

4.1 Introduction An elaborate and dedicated test program has been planned for 20MnMoNi55 which is used as RPV material. Effect of irradiation has been simulated by carrying out tensile tests at different temperatures. Since nature of the cleavage fracture has been simulated by carrying out tensile tests at different temperatures. Since nature of the cleavage fracture is inherently statistical, a large number of specimens have been tested at each temperature. Round notched tensile specimen (RNTS) have been used to impose tri-axial state of stress during testing. Figure 4.2 shows the dimensions of the specimen. It has a groove diameter of 7.7 mm and notch radius of 1.25 mm.

In all, 90 specimens (30 at each of -50 ^{0}C, -100 ^{0}C and -150 ^{0}C) have been tensile tested, using vaporized liquid nitrogen as cryogenic medium. All the experiments have been conducted under displacement controlled loading conditions. The load-displacement data were directly measured from the instrumentation provided in the machine.

Strain was applied at rate of 2 x 10^{-4} per sec. the temperature inside the experimental chamber was controlled by maintain proper flow rate of vaporize nitrogen into it, using semiconductor thermocouples and attached sensors. The loading was provided through hydraulic servo-mechanisms, using embedded control panel software.

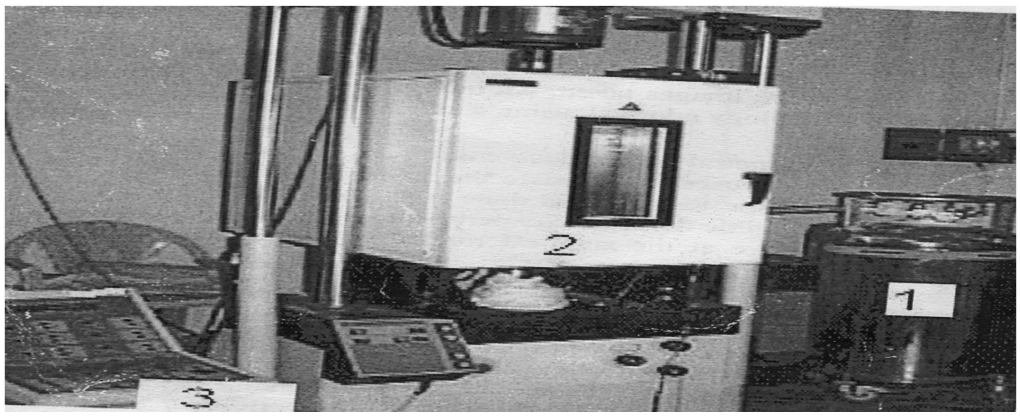

Figure 4 - 1 Experimental Setup for tensile testing (1 liquid Nitrogen, 2 Cryogenic Chamber, 3 Control Panel)

The Material used for study and experimentation is 20MnMoNi55. The Experimentation was done at BARC, Mumbai and the data was provided. The chemical composition of material and experimental setup is as follows:

4.2 Tensile Test Schedule (Material:- 20MnMoNi55)

Test Temperature	No. of Grooved Specimens	No. of Round Specimens of Uniform Gauge Diameter
-50°C	30	2
-100°C	30	2
-150°C	30	2

Table 4.1 Tensile Test Data

4.3 Chemical Composition of 20MnMoNi55

Source	C	Si	Mn	P	S	Cr	Ni	Mo	V	Cu	Al	Sn	As
[Wt-%]	0.21	0.24	1.48	0.008	0.005	0.2	0.8	0.52	0.02	0.07	0.015	0.005	0.02

Table 4.2 Chemical Properties of 20MnMoNi55

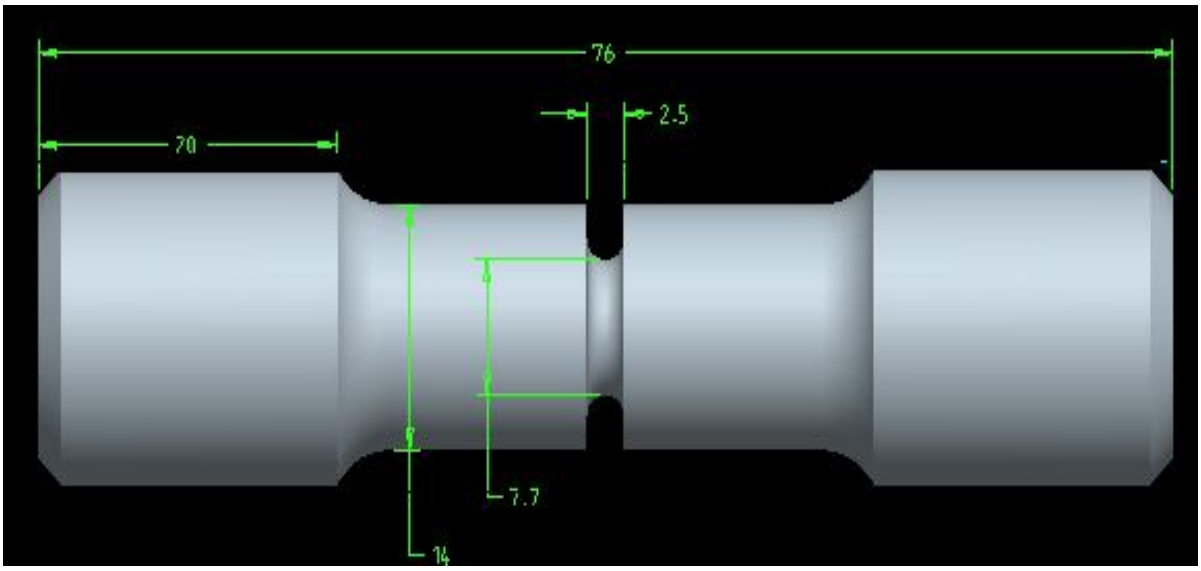

Figure 4 - 2 CAD Model and Dimensions of Grooved Specimen

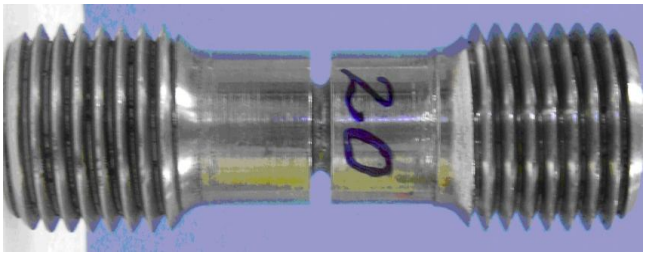

Figure 4 - 3 Grooved Specimen

Figure 4 - 4 Ungrooved Specimen

4.4 Experimental Data

Experimental Data for temperatures -50, -100 and -150 ^{0}C is given below:

S. No.	Sample No.	Initial Diameter (mm)	Diametrical Contraction (mm)	Peak Load (kN)	Breaking Load (kN)
1	9	7.78	-------	50.2	41.3
2	8	7.8	-------	50.91	41.42
3	73	8.04	1.49	51.94	41.23
4	74	8.02	1.41	54.4	44.21
5	75	8.04	1.61	54.03	42.49
6	76	8.04	1.43	53.48	42.07
7	78	8.03	1.44	55.73	45.38
8	79	8.05	1.50	55.35	43.6
9	82	7.82	1.41	51.76	42.01
10	83	7.82	1.31	53.65	43.56
11	84	7.86	1.33	51.64	41.78
12	85	7.86	1.39	52.69	43.01
13	86	7.85	1.37	52.72	42.33
14	87	7.83	1.38	53.46	42.96
15	88	7.85	1.36	53.07	42.57
16	89	7.85	1.33	51.84	42.04
17	90	7.87	1.77	52.55	42.19
18	91	7.87	1.48	52.61	42.56
19	92	7.85	1.35	52.88	43.76
20	93	7.79	1.42	52.73	42.34

21	94	7.85	1.60	52.15	41.52
22	95	7.86	1.63	53.11	42.28
23	96	7.86	1.52	51.87	40.18
24	98	7.86	1.47	51.52	40.37
25	99	7.84	1.44	54.49	43.36
26	100	7.86	1.58	52.08	41.80
27	101	7.85	1.37	52.1	42.03
28	102	7.92	1.48	53.32	43.55
29	103	8.04	1.43	54.73	44.91
30	104	7.84	1.54	52.58	40.71

Table 4.3 : Summary of Tensile Test Results on 30 Grooved Samples at -50 ^{0}C

S. No.	Sample No.	Initial Diameter (mm)	Diametrical Contraction (mm)	Peak Load (kN)	Breaking Load (kN)
1	80	7.83	1.443	57.63	48.2
2	105	7.85	1.5493	57.58	46.67
3	106	7.84	1.5246	56.66	46.48
4	107	7.86	1.5269	58.31	48.65
5	108	7.85	1.4106	56.7	46.84
6	110	7.83	1.4925	55.89	44.81
7	111	7.85	1.4636	56.36	46.15
8	112	7.74	1.5299	56.88	46.11
9	113	7.83	1.3989	56.76	48.14
10	114	7.89	1.4956	55.76	45.90
11	115	7.84	1.5194	54.41	43.06
12	116	7.99	1.5080	57.68	47.92
13	117	7.86	1.5219	57.41	47.22
14	118	7.85	1.3521	58.81	46.87

15	120	7.81	1.4198	57.21	47.61
16	121	7.85	1.7265	57.58	46.73
17	122	7.92	1.2305	61.29	53.74
18	124	7.83	1.2429	58.68	47.76
19	125	7.86	1.4859	58.27	50.42
20	126	7.87	1.479	60.05	50.36
21	127	8.04	1.5284	57.97	47.59
22	129	7.99	1.5212	60.67	50.28
23	130	7.95	1.6262	58.91	47.58
24	132	7.86	1.3915	58.68	49.21
25	133	7.86	1.3873	60.28	50.35
26	134	7.99	1.593	59.15	47.83
27	135	7.88	1.446	58.31	49.22
28	136	7.84	1.4324	56.33	48.88
29	137	7.84	1.2513	57.09	48.76
30	155	7.80	1.5199	56.28	44.92

Table 4.4 : Summary of Tensile Test Results on 30 Grooved Samples at -100 ^{0}C

S. No.	Sample No.	Initial Diameter (mm)	Diametrical Contraction (mm)	Peak Load (kN)	Breaking Load (kN)
1	81	7.99	1.1408	67.59	63.25
2	140	7.81	0.7171	64.24	63.3
3	142	7.9	0.4252	67.72	67.58
4	145	7.78	0.681	63.59	62.95
5	146	7.77	-	67.50	67.50
6	147	7.76	-	65.48	64.78
7	148	7.76	0.7052	63.97	62.93
8	149	7.77	0.7296	64.98	64.07

9	150	7.79	0.7065	63.84	62.36
10	151	7.75	0.7329	63.4	62.16
11	152	7.74	0.6219	63.84	63.39
12	153	7.79	0.6192	65.88	64.56
13	154	7.77	0.6985	64.9	63.64
14	161	7.78	1.088	64.17	54.64
15	162	7.79	0.7926	63.22	61.27
16	164	7.81	0.8546	64.64	64.14
17	165	7.76	0.5424	64.56	63.48
18	166	7.75	0.3953	64.62	64.41
19	167	7.78	0.8323	64.12	62.58
20	168	7.75	0.9261	61.63	58.62
21	169	7.68	0.6961	62.76	61.8
22	170	7.78	0.7505	65.05	63.64
23	171	7.7	0.9669	64.5	61.21
24	172	7.78	0.2151	63.57	63.5
25	173	7.82	0.6334	64.22	64.95
26	175	7.76	0.6372	64.98	64.27
27	178	7.8	0.4009	64.79	64.71
28	180	7.76	0.9914	65.11	62.19
29	182	7.79	0.1927	60.81	60.8
30	183	7.74	0.1933	62.3	62.08

Table 4.5 : Summary of Tensile Test Results on 30 Grooved Samples at -150 ^{0}C

S. No.	Sample No.	Test Temperature (^{0}C)	Initial diameter (mm)	Axial Extension (mm)	Peak load (kN)	Breaking load (kN)
5	L 10	-50	6.02	7.549	20.310	12.620
6	L13	-50	6.07	6.992	20.320	12.420
7	L 09	-100	5.95	8.014	21.810	13.870
8	L 15	-100	5.90	6.946	21.008	13.375
9	L 14	-150	5.98	7.014	23.668	15.516
10	L11	-150	6.07	6.882	24.330	17.210

Table 4.6 : Summary of Tensile Test Results On Un grooved Samples At Different Test Temperatures

4.5 Experimental Load VS. Axial Displacement Plots

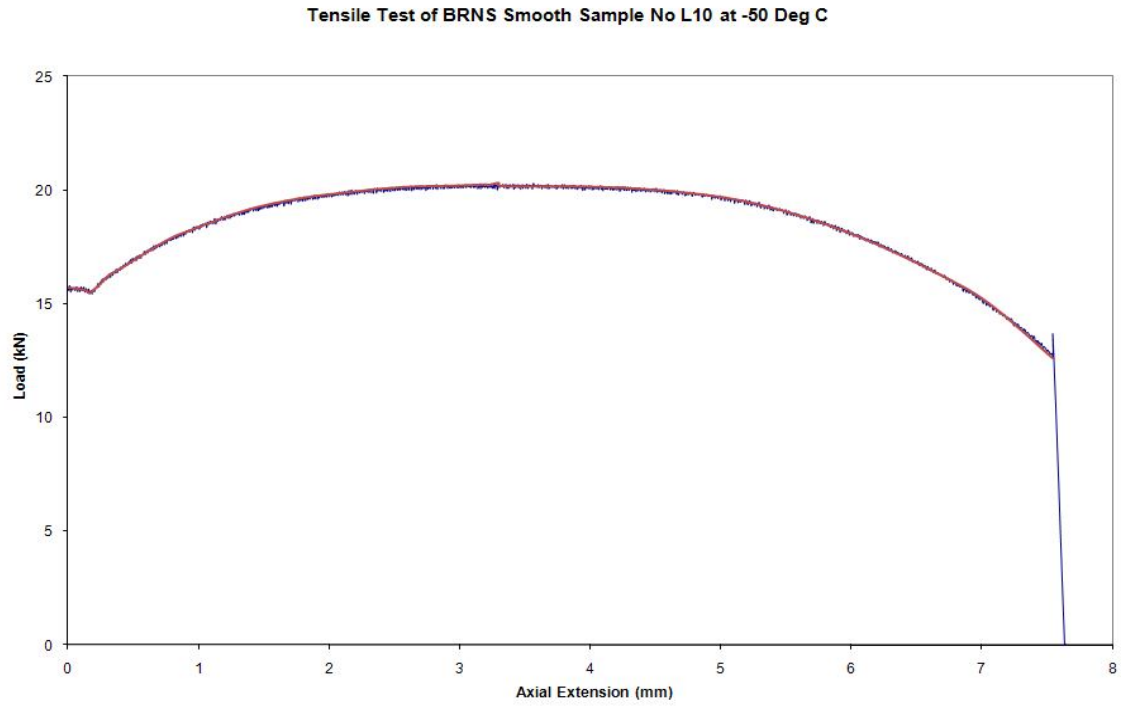

Figure 4 - 5 Axial Load vs. Displacement Curve of Sample No. L10 at -50 ^{0}C

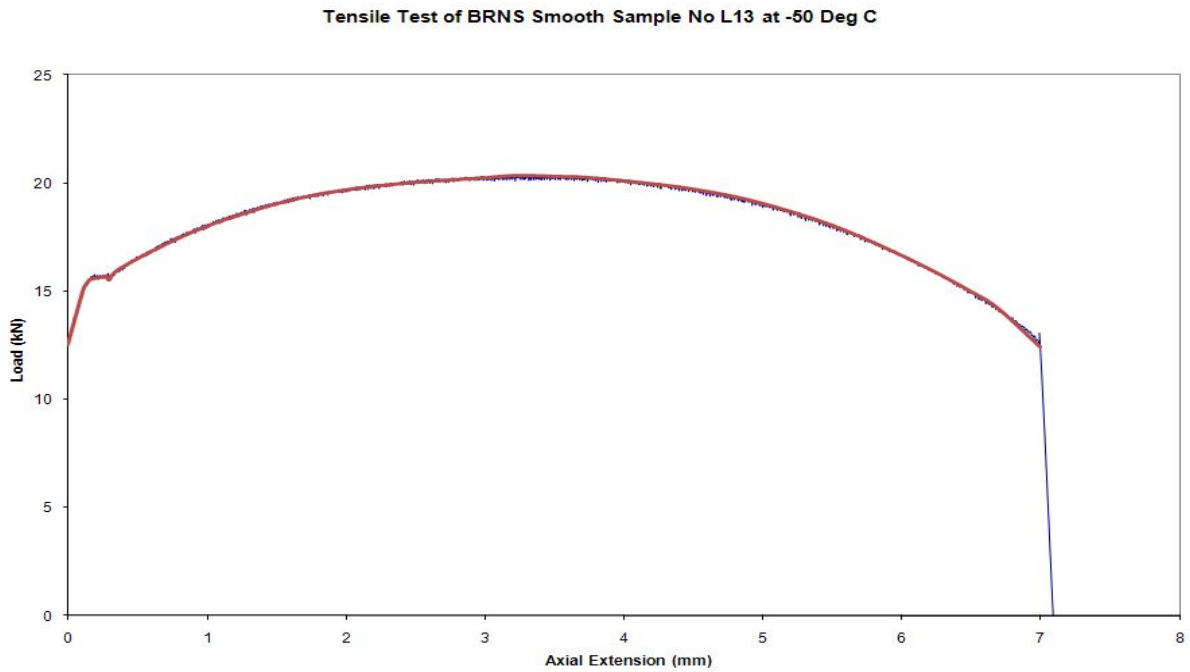

Figure 4 - 6 Axial Load vs. Displacement Curve of Sample No. L13 at -50 ^{0}C

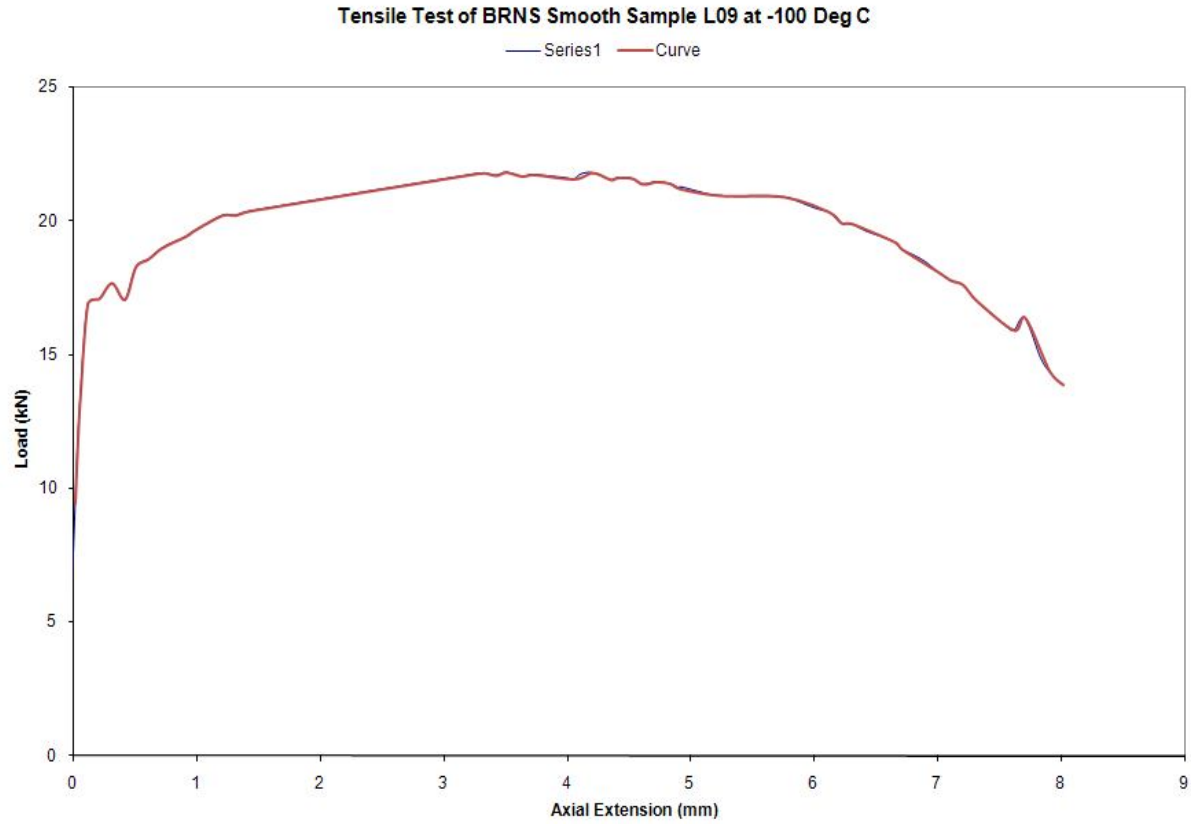

Figure 4 - 7 Axial Load vs. Displacement Curve of Sample No. L09 at -100 ^{0}C

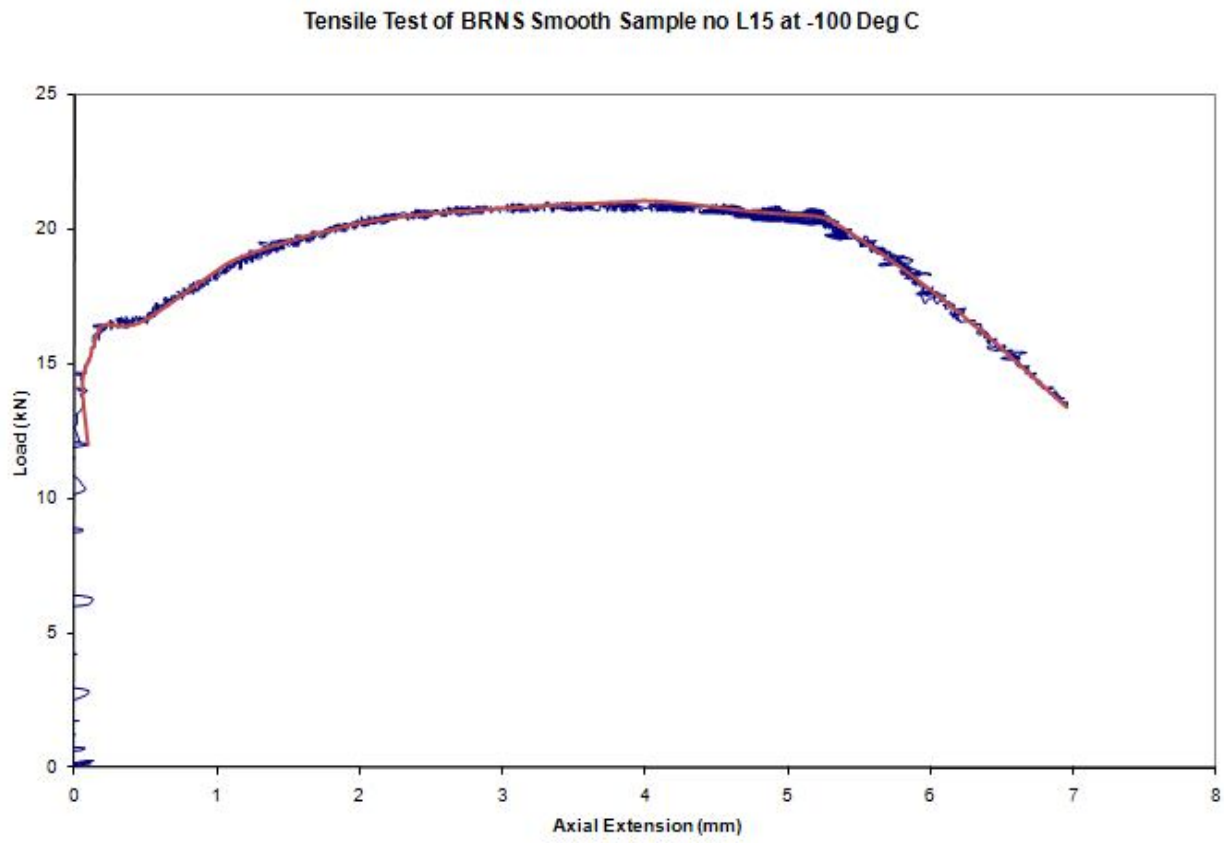

Figure 4 - 8 Axial Load vs. Displacement Curve of Sample No. L15 at -100 ^{0}C

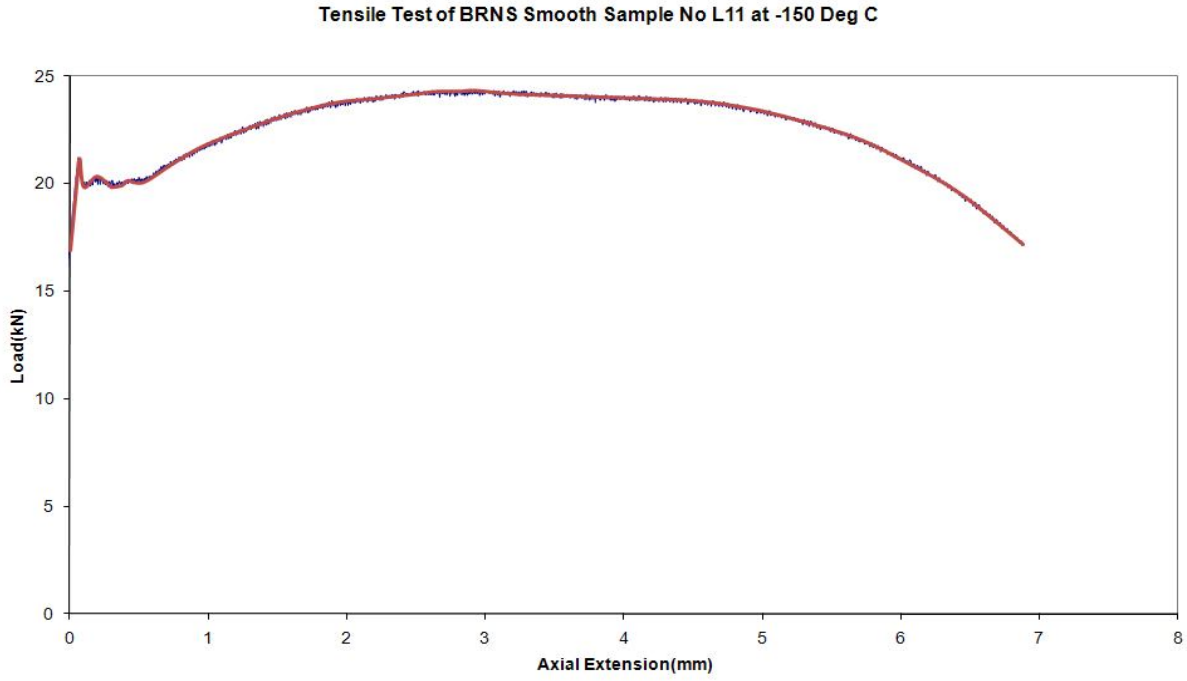

Figure 4 - 9 Axial Load vs. Displacement Curve of Sample No. L11 at -150 ^{0}C

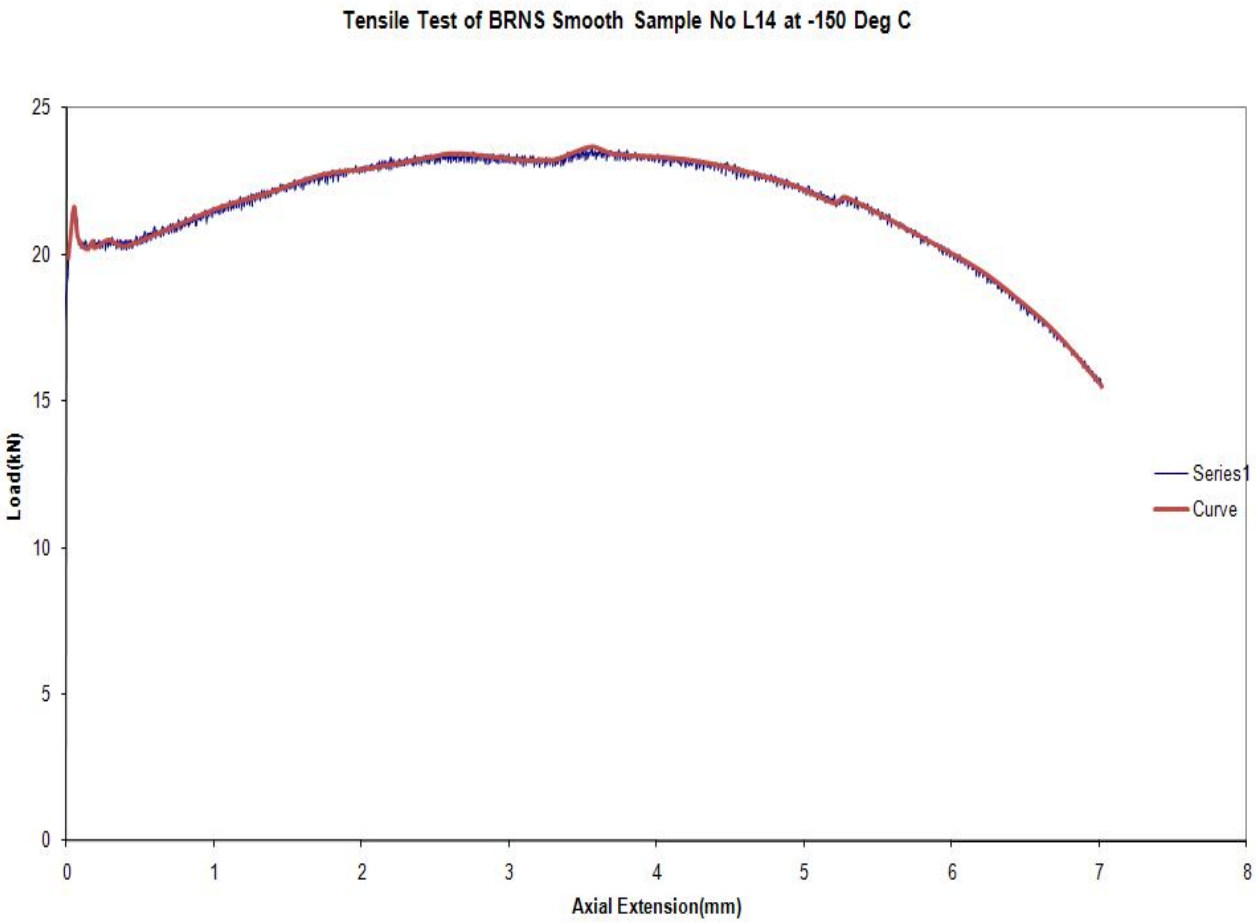

Figure 4 - 10 Axial Load vs. Displacement Curve of Sample No. L14 at -150 ^{0}C

4.6 Calculation of Stress VS. Strain Data From Experimental Results

To obtain Stress Strain relation from experimental data the following procedure was done:

1 Calculate the Engineering Stress Strain from Experimental data using formulae:

$$\epsilon_e = \frac{\delta l}{l_0}$$

2 Calculate the True Stress Strain from Engineering Stress Strain using formulae:
The Experimental Stress Strain data is extrapolated using equation of Power law given below-

3 Strain Hardening of material due to plastic deformation should be compensated, this is done by using power law equation given below
Extrapolation of Stress vs. Strain data using A, n = Constants
following :

(Power Law)

Taking log of above equation both sides -

$$\text{Log}\,(\sigma_p) = \log\,(A) + n \log\,(\epsilon) \qquad \text{(Taking log both sides)}$$

Now we can see that above equation is equation of straight line with slope 'n' and intercept log(A), thus for extrapolation of experimental stress strain data beyond ultimate strength point, a straight line is fitted in data from elastic limit to ultimate point, and then stresses can be calculated using slope and intercept obtained from straight line fit. The straight line fit values of slope and intercept for un-grooved samples at different temperatures are given in table below:-

4.7 Stress VS. Strain Relationship And Plots At Tested Temperatures

Test Temperature	Sample No.	Slope (n)	Intercept Log(A)	Equation
-50 Deg.	L10	0.15397	3.04616	$\mathrm{Log}\,(\sigma_p) = 3.04616 + 0.15397 * \log(\epsilon)$
-50 Deg.	L13	0.17725	3.06180	$\mathrm{Log}\,(\sigma_p) = 3.06180 + 0.17725 * \log(\epsilon)$
-100 Deg.	L09	0.15577	3.08737	$\mathrm{Log}\,(\sigma_p) = 3.08737 + 0.15577 * \log(\epsilon)$
-100 Deg.	L15	0.17795	3.09078	$\mathrm{Log}\,(\sigma_p) = 3.09078 + 0.17795 * \log(\epsilon)$
-150 Deg.	L11	0.16218	3.12781	$\mathrm{Log}\,(\sigma_p) = 3.12781 + 0.16218 * \log(\epsilon)$
-150 Deg.	L14	0.12885	3.08960	$\mathrm{Log}\,(\sigma_p) = 3.08960 + 0.12885 * \log(\epsilon)$

Table 4.7 Stress vs. Strain Relationship of 20MnMoNi55 at different test temperatures

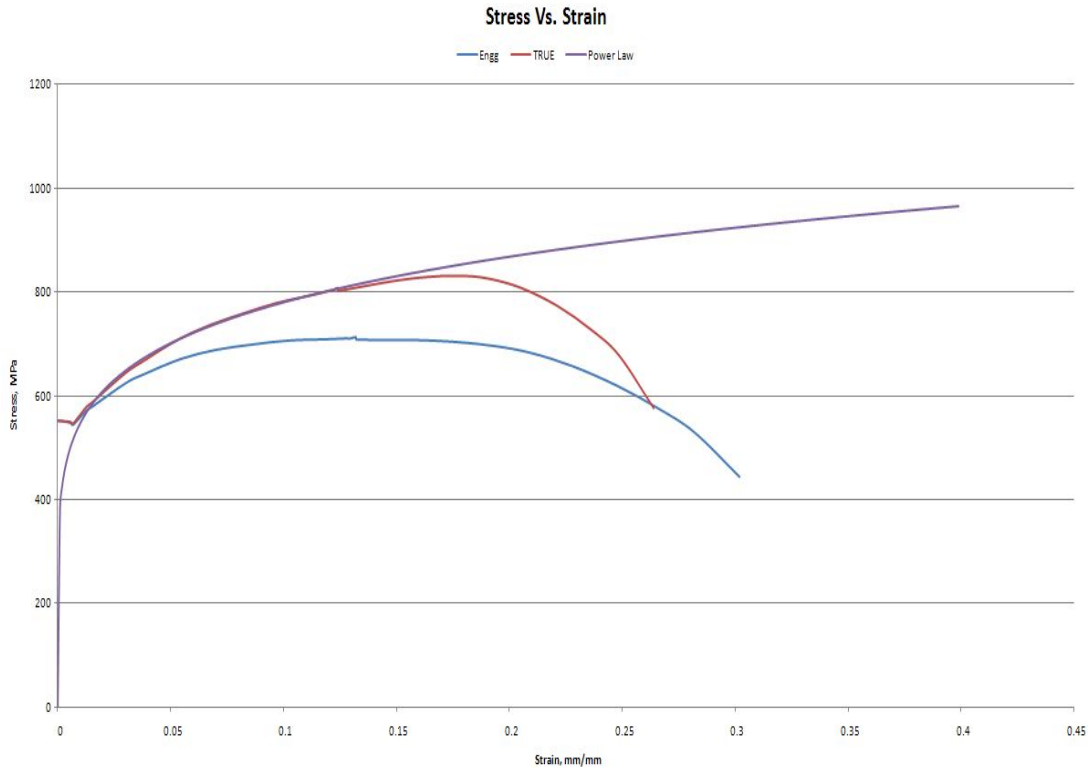

Figure 4 - 11 Stress vs. Strain Plot of Sample L10 at -50 0C

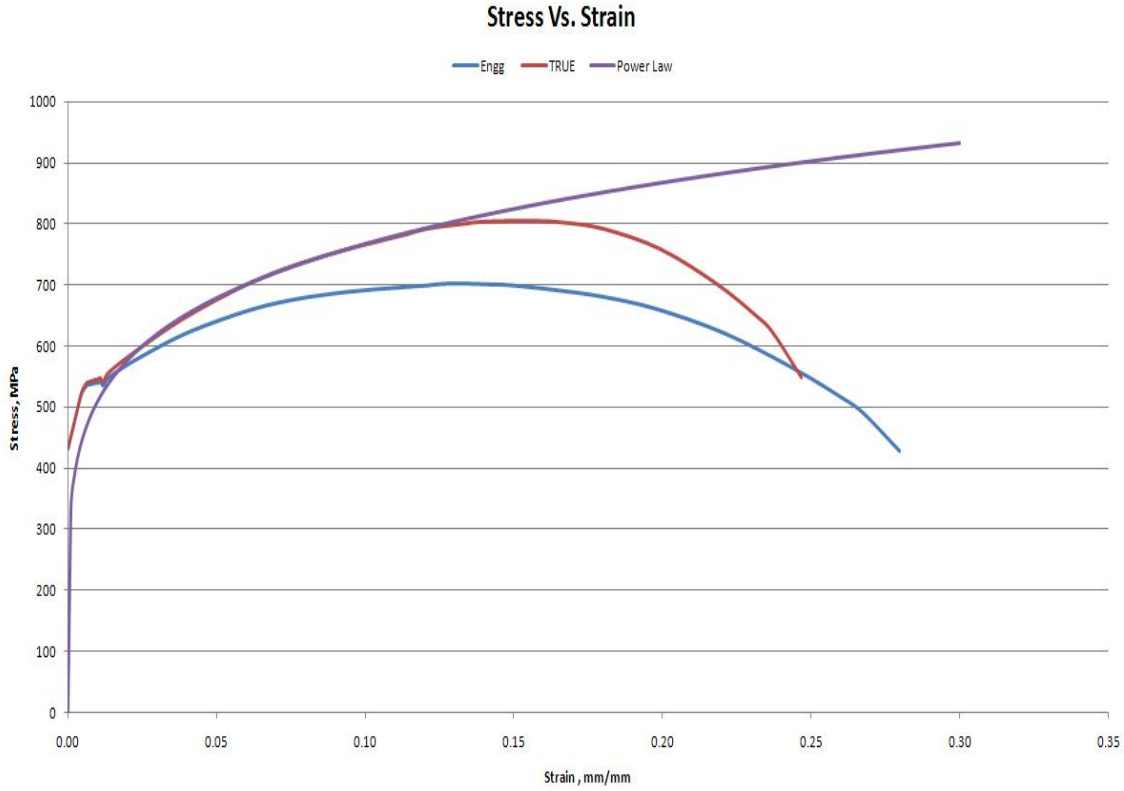

Figure 4 - 12 Stress vs. Strain Plot of Sample L13 at -50 0C

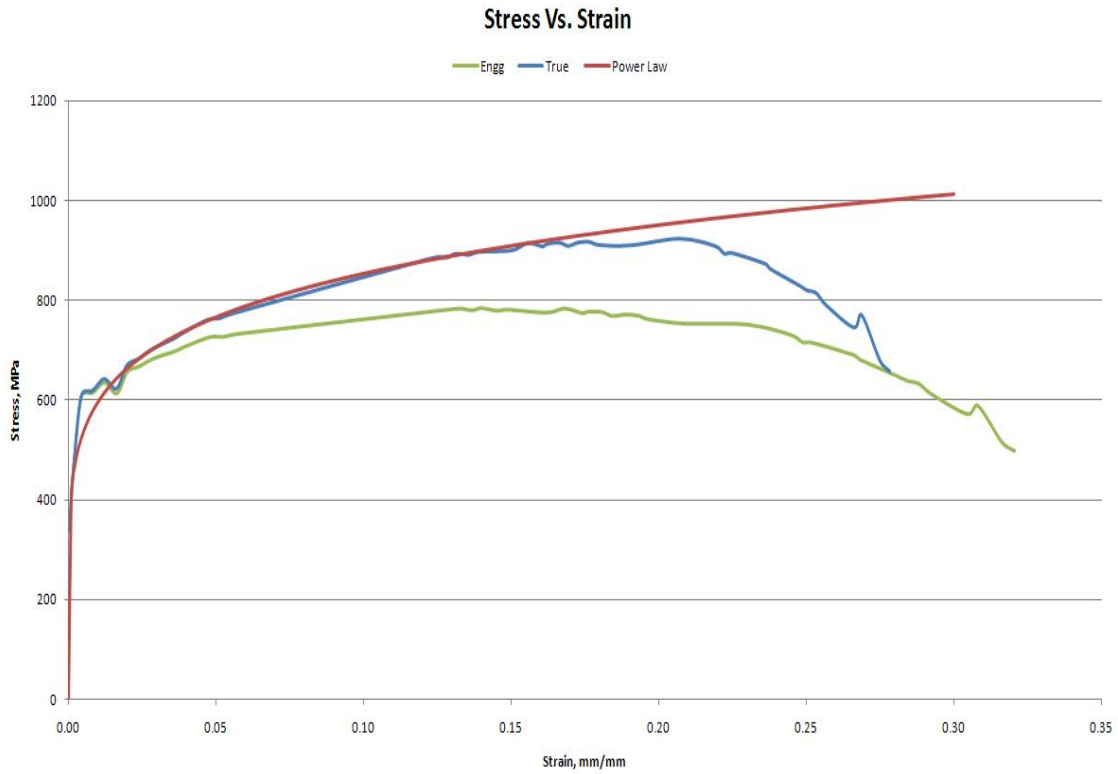

Figure 4 - 13 Stress vs. Strain Plot of Sample L09 at -100 0C

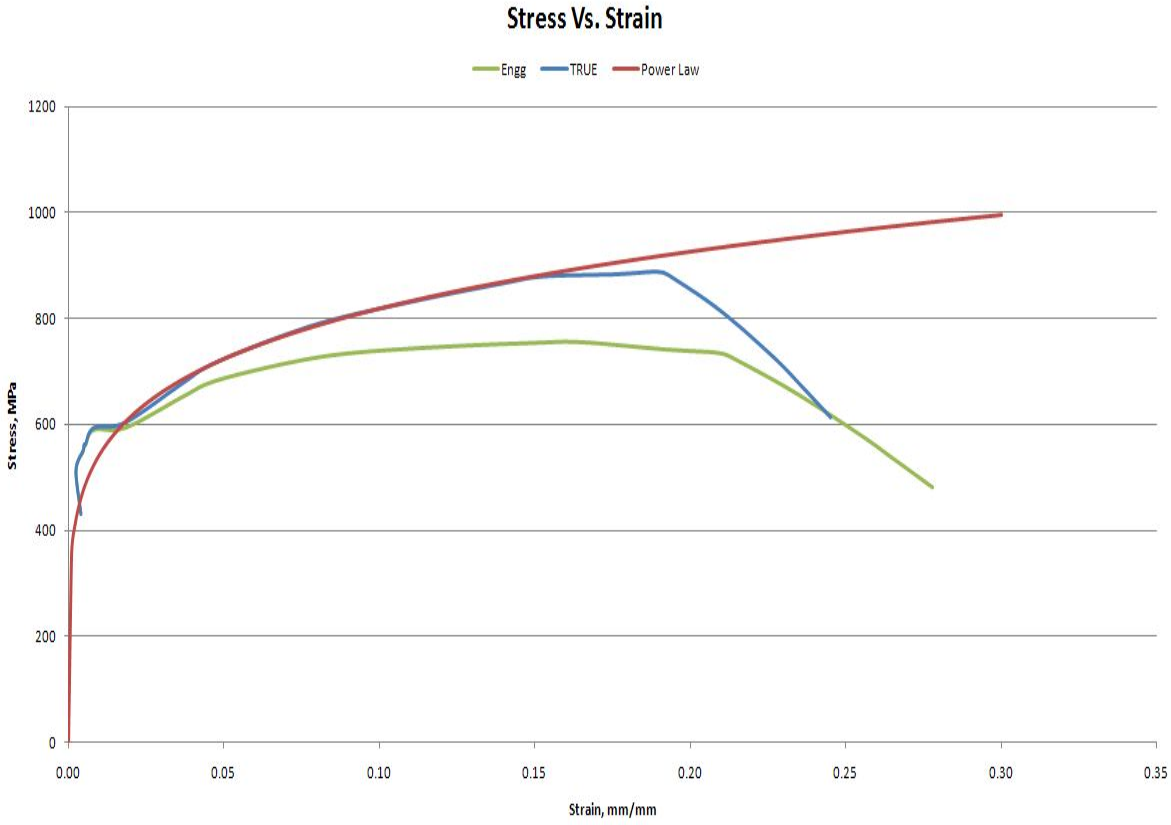

Figure 4 - 14 Stress vs. Strain Plot of Sample L15 at -100 0C

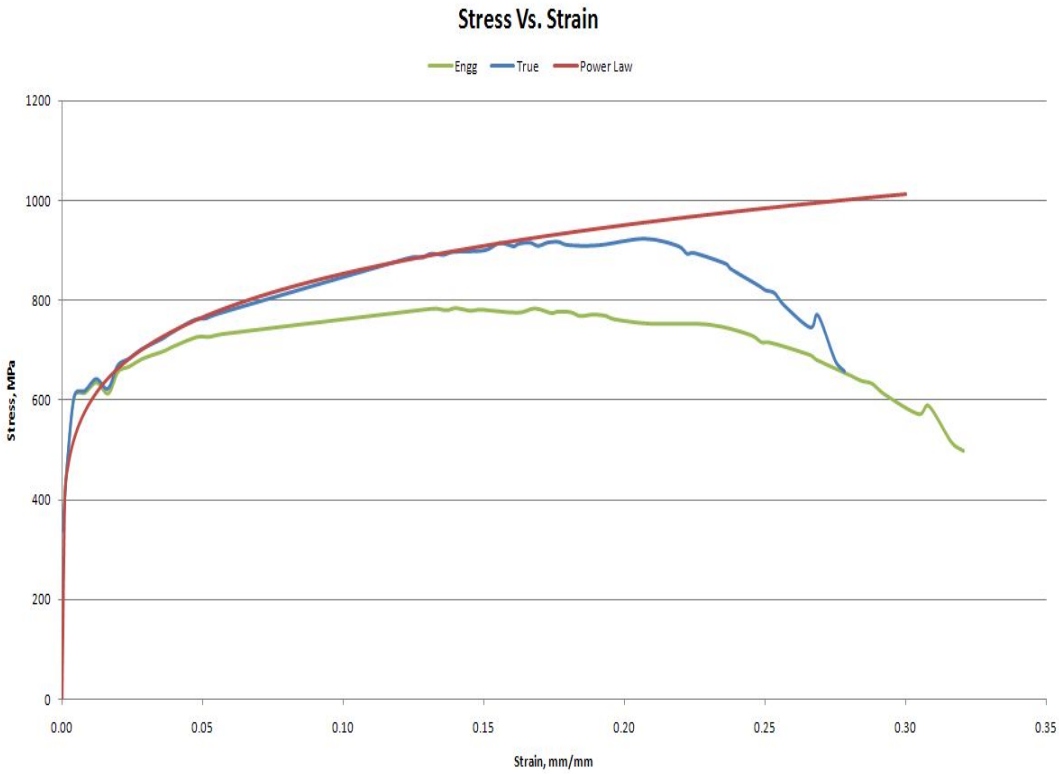

Figure 4 - 15 Stress vs. Strain Plot of Sample L11 at -150 0C

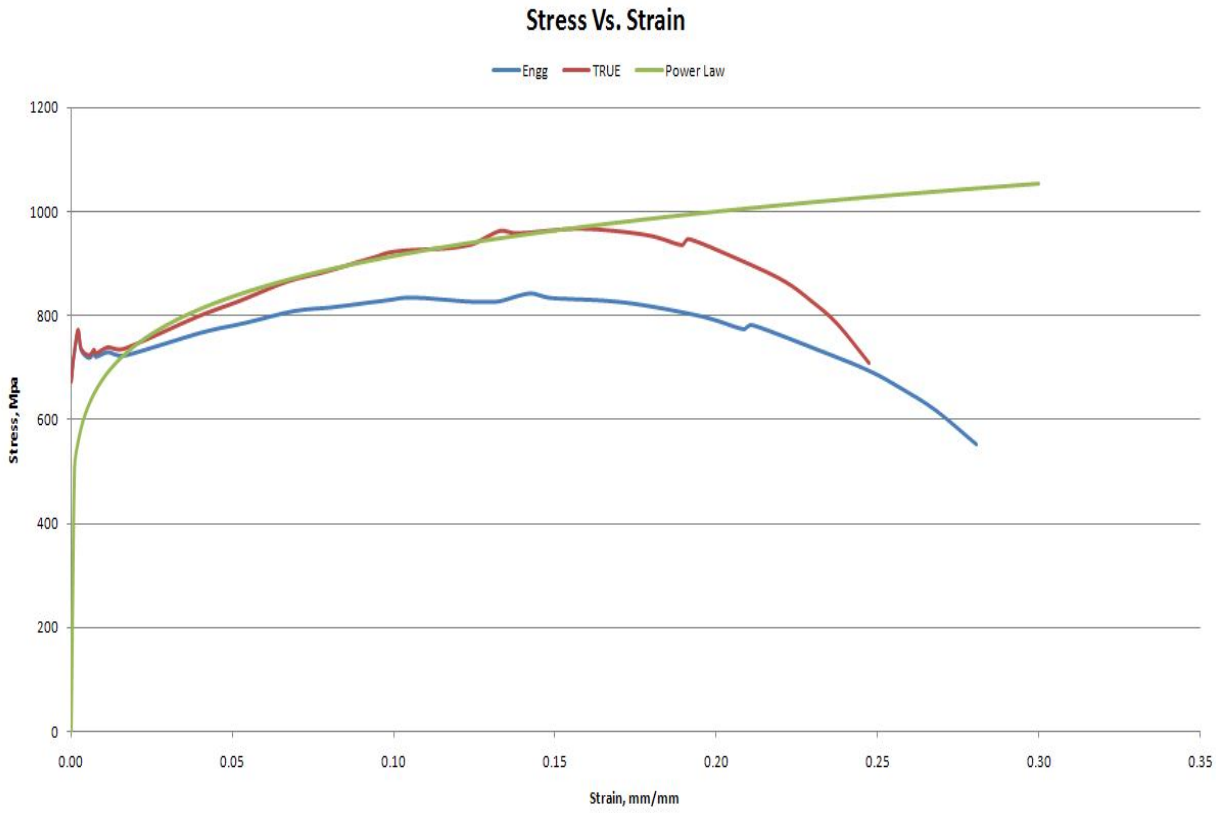

Figure 4 - 16 Stress vs. Strain Plot of Sample L14 at -150 0C

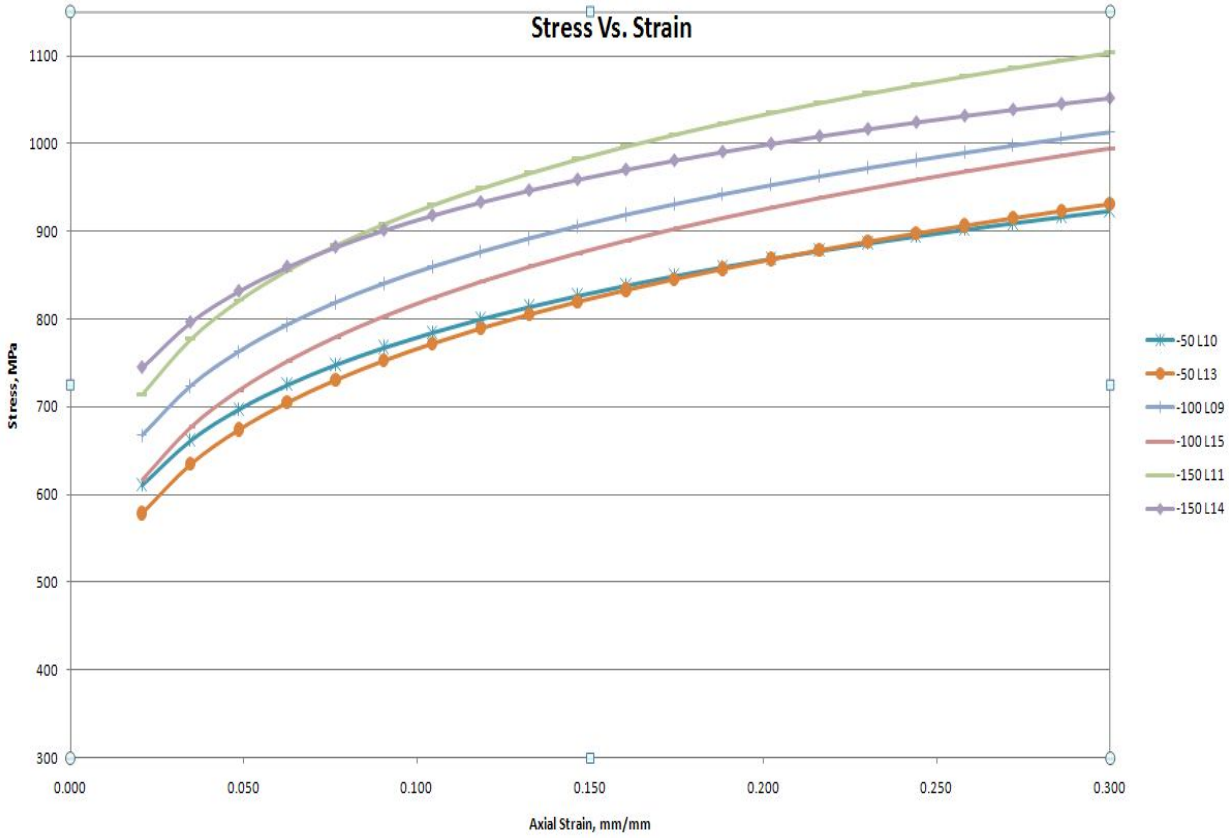

Figure 4 - 17 Stress vs. Strain Plots of 20MnMoNi55 at -50 ,-100, -150 ^{0}C

CHAPTER - 5

FE Analysis and Post Processing

5.1 Overview

The following flow chart shows Methodology followed to determine the Beremin's Parameters:

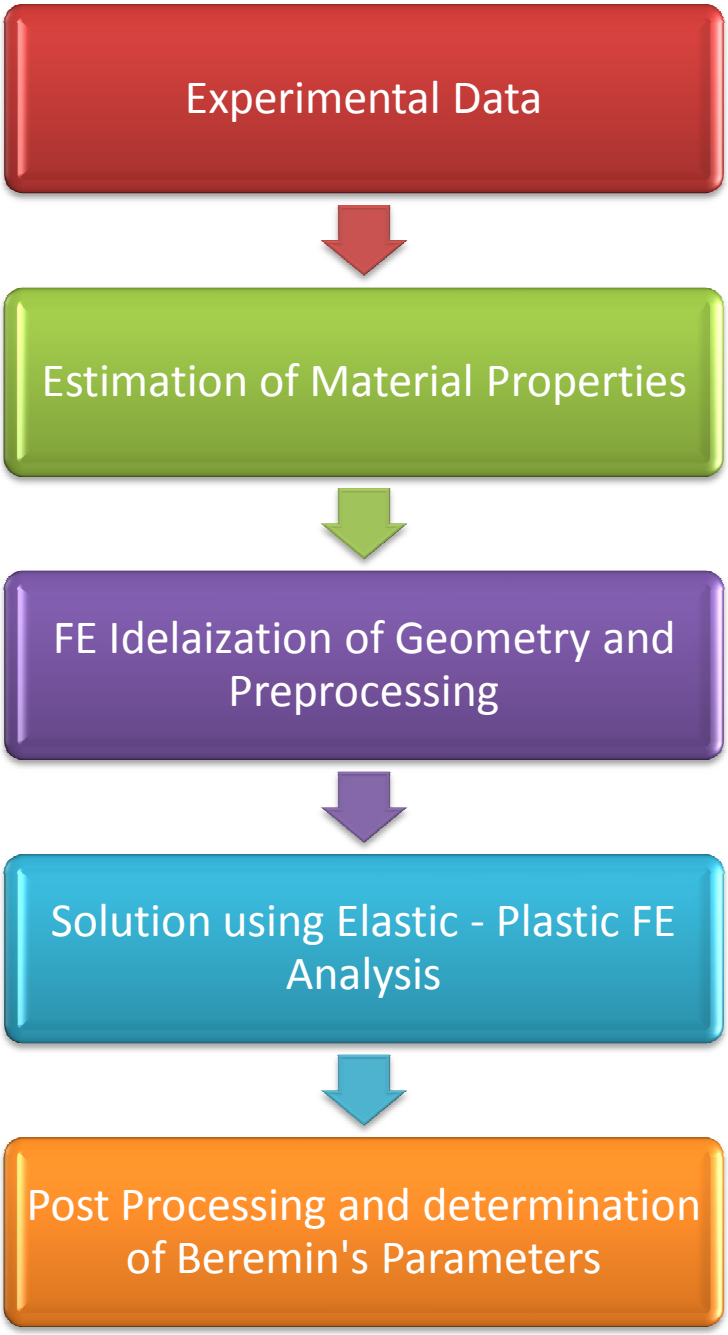

Figure 5 - 1 Methodology followed for the Estimation of Beremin's parameters

Figure 5 - 2 Process Chart for determination of Beremin's parameters used by author

5.2 Pre-Processing

5.2.1 Geometric Idealization

As during the Tensile Testing of Specimens only Uniaxial Tension was applied and also the geometry of Specimens used for testing was symmetric, therefore to reduce computational time and storage required for Finite Element Analysis purposes the model was idealized to 2-D Model and only $1/8^{th}$ model of actual test specimen was modeled. An 8 node iso-parametric Element is used for meshing the geometry of specimen. For finding out accurate results and reducing Analysis time different sizes of meshing are used in FE model of Specimen, a finer mesh is used in near groove region, the mesh size near the groove region ranges from 46 μm to 49 μm and coarse mesh is used in less significant region of specimen and to combine both regions transition element are used to ensure the proper connectivity. The images of complete mesh is shown in Figure 4.3 and a zoom view of finer mesh also is shown in Figure 5.4

5.2.2 Geometric Modeling And Meshing

Geometric modeling and meshing is done using popular FEA software ANSYS and geometry and FE data exported to ‘ cdb ‘ file. Since diameters of all specimens tested were not identical, therefore to reduce modeling and meshing time of specimens having identical geometrical features, except diameter of grooved region specimen a parametric model was modeled using APDL (ANSYS Parametric Design Language). The code for parametric model is capable of geometric modeling and meshing of specimen by taking ‘ Specimen Number ’ and ‘ Initial Diameter ’ from user and giving output as ANSYS database file and ‘.cdb’ file placed in directory named as specimen number in the current working directory.

5.2.3 Madam Input Format And Input File Generation

Another code named ‘ **A2M** ‘ was developed for the preparation of input file for the BARC In-House FEA code MADAM (Material Damage Modeling) for Elasto-Plastic FEA analysis of specimen, the inputs required for A2M are material properties(yield strength, Poisson ratio, young’s modulus and material stress vs. strain curve based on experimental data) , ANSYS exported ‘ .cdb ‘ file and few other

inputs(i.e. Solver to be used, no. of Gauss points to be used etc.). The output file of A2M can be directly used for MADAM input file without any need of further editing. The complete MADAM input format is as follows:

MADAM INPUT FORMAT

Card 1	First word (A10):	Name of equation solver- ➢ SPRASE ➢ FRONTAL ➢ COLSOL (column solver) ➢ LPCG (linear pre-conditioned conjugate gradient solver)
	Second word (A10):	Solution technique- ➢ NEWTON (Newton-Raphson method) ➢ RIKS (Modified Rik's method)
	Third word (A10):	Integration scheme employed- ➢ MIDPOINT ➢ BEULER (backward Euler) ➢ FEULER (forward Euler)
Card 2	This card set (A80)	Describes Title to the problem.
Card 3	First data (I5):	Total number of elements
	Second data (I5):	Total number of nodes
	Third data (I5):	Total number of nodes per element
	Fourth data (I5):	Number of elements for which the node relations are to be provided
	Fifth data (I5):	Number of nodes for which the coordinates are to be provided Sixth data (I5):–
	Sixth data (I5):	Index for loading condition 1 (Plane stress) 2 (plane strain) 3 (axis- symmetric case)

4 (3-D case)

Card 4	First data (I5):	Number of materials
	Second data (I5):	Type of stress strain curve- 1 - (true stress- true strain) 2 - (engineering stress engineering strain)
	Third data (I5):	Type of analysis- 0 (elastic –plastic) 12 (damage mechanics)
	Fourth data (I5):	Index for material hardening- 0 - (isotropic hardening) 1 - (kinematics hardening
Card 5	First data (I5):	Number of group of boundary conditions
	Second data (I5):	Total number of boundary nodes
	Third data (I5):	Number of group of loads
Card 6	First data (I5):	Index for geometric non-linearity-1(On), 0(Off)
	Second data (I5):	Number of load increments
	Third data (I5):	Maximum number of iteration for convergence
	Fourth data (I5):	Number of group of load fractions
	Fifth data (I5):	Number of print interval for output files.
Card 7	Here element and node relationship is provided which has been obtained through the mesh generating code or software.	

For 2D 4-node iso- parametric quadrilateral element

First data (I5):	Elements ID
Second data (I5):	Material ID
Third to sixth data (I5):	ID of corner nodes

For 2D 8-node iso- parametric quadrilateral element

First data (I5):	Elements ID
Second data (I5):	Material ID
Third to sixth data (I5):	ID of corner nodes (anticlockwise)
Seventh to tenth data (I5):	ID of corresponding mid - nodes (anticlockwise)

For 3D 20-node brick element

First data (I5):	Elements ID
Second data (I5):	Material ID
Third to tenth data (I5):	ID of corner nodes
Eleventh to 18th data (I5):	ID of corresponding mid - nodes

Card 8 Here the co-ordinates in x, y and z direction for each node are provided as obtained through the mesh generating code or software.

Card 9 Depending upon the number of groups of boundary conditions data are to be provided in this card.

Card 10 In this card material properties are given.

First data (E10.3):	young's modulus of elasticity in MPa of material
Second data (E10.3):	Poisons ratio
Third data (E10.3):	Yield stress
Fourth data (I5):	Number of data points for stress strain curve

Card 11 This card gives the data for stress-strain curve and immediately follows the card where young's modulus is provided.

Card 12 This card is only to be read when the 3rd data in 4th card is 1. The data are Gurson parameters.

Card 13 This card gives number of group of distributed loads and number of concentrated loads. For displacement controlled loading these parameters are zero.

Card 14 This card is read only when first data in card 13 is non zero. This card provides data for each face.

Card 15 This card is read only when second data in card 13 is non zero. It provides data regarding node number and corresponding loads in x and y direction.

Card 16 Depending on the no. of group of loads and the number of groups of load fraction data is to be provided.

Card 17 Here the data represents no. of elements for which damage mechanics calculations is to be done.

Card 18 The data in this card represents the id of elements for which damage mechanics calculation is required.

Card 19 This card gives data regarding engineering quantity to be found (displacement, reaction etc.) and range of nodes for which it is to be found.

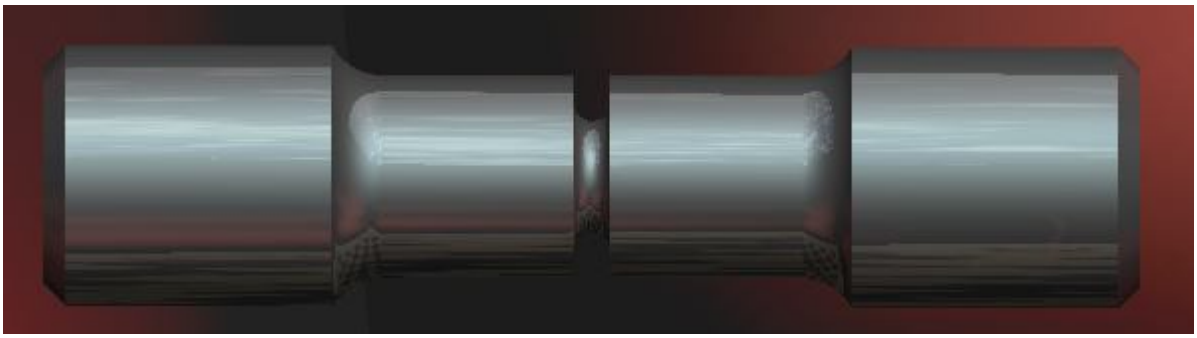

Figure 5 - 3 Actual Geometry of Specimen

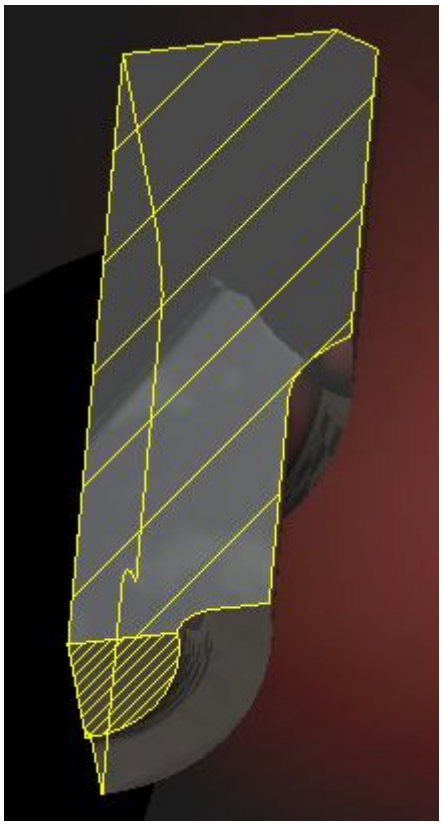

Figure 5 - 4 Cut Section of 1/8th model of actual grooved specimen

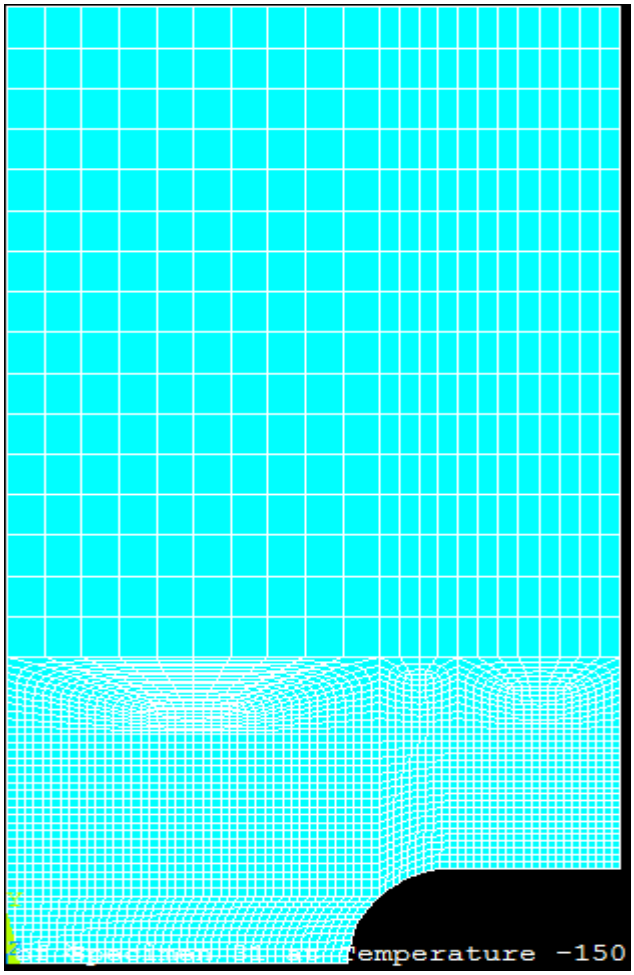

Figure 5 - 5 Idealized 2-D Mesh used for FE Analysis

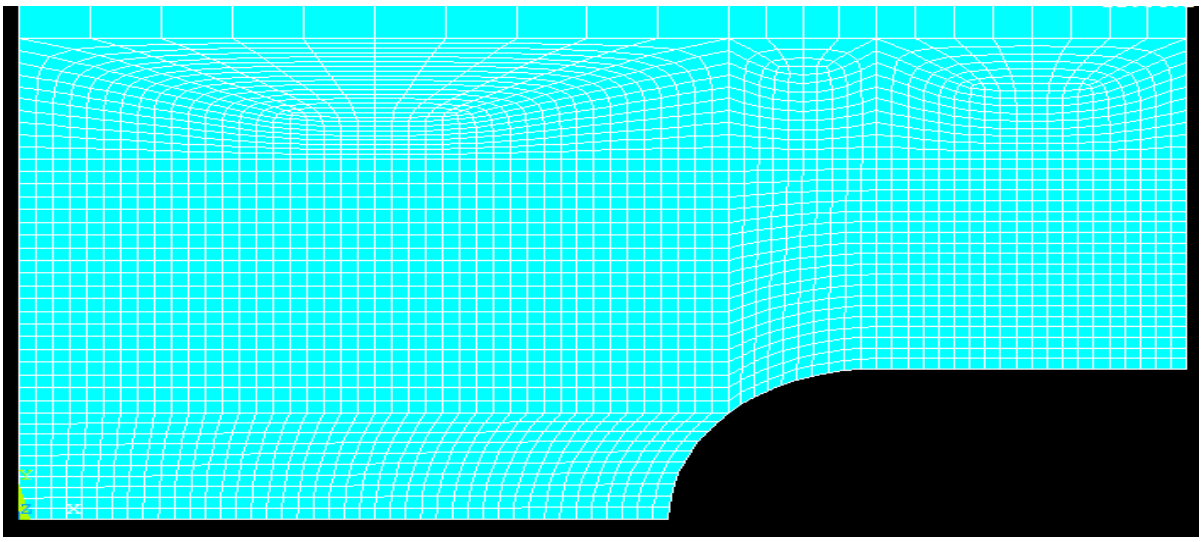

Figure 5 - 6 Zoom view of Fine mesh near groove region

5.3 Solution And Post Processing

To obtain the Stress-Strains, nodal reactions and nodal displacements value of an Elastic-plastic FE analysis BARC In House Code **MADAM** (Material Damage Modeling) was used. The details of solution and post processing are as follows:

5.3.1 Running FE Analysis Using Barc In House Code Madam

- A2M generated MADAM inputs file were used to run the MADAM code for the Finite Element Analysis of the specimen geometry and loading conditions.
- The Parameters used for Analysis were:
- Simultaneous Equation Solver: SPARSE
- Solution Technique: NEWTON
- Integration Scheme Employed: MIDPOINT
- Element Type: 8-noded Iso-Parametric
- Type of Analysis: 2D Axisymmetric Elastic-Plastic
- Boundary Conditions: Y- fixed at base, X- fixed along the axial axis, displacement prescribed on top edge
- Stress Strain Curve: True Stress Strain
- Young's modulus and Poisson ratio: 2.1×10^5 MPa and 0.3 respectively
- Yield Strength: As per experimental results for different temperatures
- Load Step: 0.005 mm

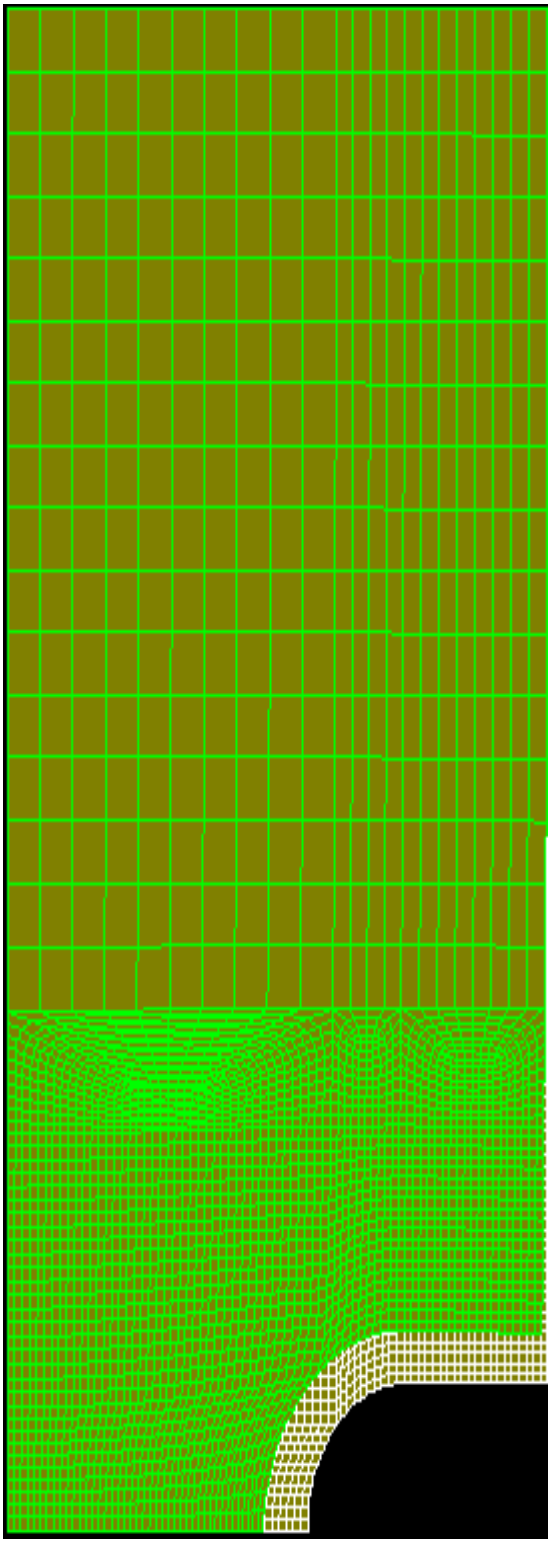

Figure 5 - 7 Initial and Deformed geometry after FE analysis

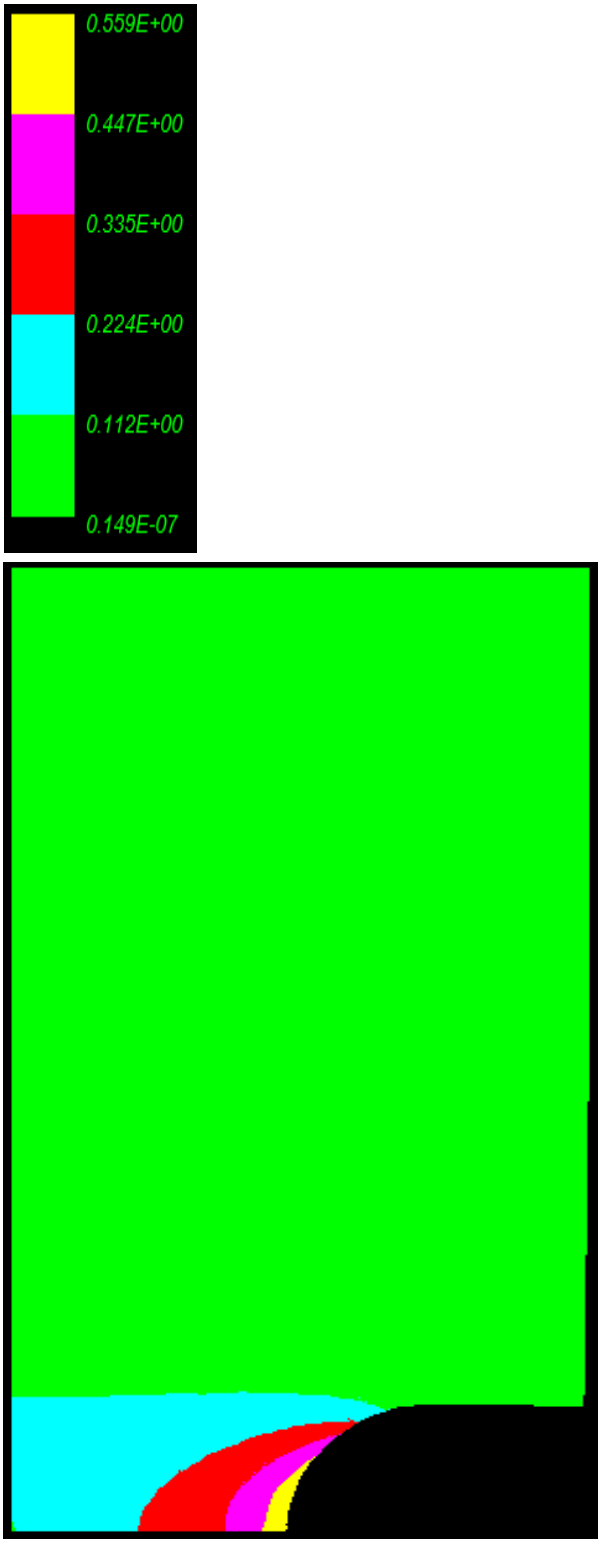

Figure 5 - 8 Contour Plot of Plastic Strains from FEA

5.4 Post Processing:

1. MADAM.DAT: In this file values of Nodal displacements, Stresses, Strains and Nodal Reactions for after specified load step interval are stored.

2. MADAM-POST.OUT : Stores in detail the deformation history and different stress and strain values.

3. *.OUT: Gives the damage elements corresponding iteration number and gauss point and also confirms the input data

5.4.1 Post- Processing For Load & Diametrical Contraction (ΔD) Data:

A post processor named as 'LDPLOT' was developed to obtain Diametrical Contraction (ΔD) and Load from the FEA results. The output file contains data Maximum load occurred during FEA analysis, the node number used to calculate diametrical contraction for the particular specimen geometry in experimentation, and load step and corresponding ΔD and load. These values are used to plot Load vs. ΔD curves.

5.4.2 Post- Processing For Beremin's Parameters:

Another post processor named as 'BERMINPAR' was developed to determine Beremin parameters σ_u and m. for the RPV material 20MnMoNi55 at different cryogenic temperatures based on experimental results and FE Analysis. Beremin parameters were calculated using "Maximum Likely-hood Method" (See Appendix 1) by taking experimental load at fracture as ranking parameter. The V_0 for 20MnMoNi55 was taken as 0.001 mm^3. The initial guessed value for iterative loop was taken as 22.

5.5 Results & Discussions

The material investigated was a German Nuclear Reactor Pressure steel (20MnMoNi55). The notched tensile specimens were taken from different positions of the material block. The experimental load displacement curve for the specimens having same configuration varied depending upon position of the specimens in the material block. The notched tensile specimens were analyzed with the help of an In house finite element code MADAM. The difference in fracture points are because of the fact that process of cleavage fracture follows Weibull statistical distribution the two Weibull parameters m and σ_u are material properties and varies from material to material. Here we have determined these two parameters by maximum likely-hood method by taking fracture load as the ranking parameter of the specimens.

The **Load vs. ΔD** plots obtained using FE analyses are shown below, which are as expected. The Beremin's parameters found are tabulated in table form and **P_f vs. σ_w** plots are also shown below. Since material properties were determined from two ungrooved samples tested at each temperatures therefore each Load VS. ΔD plot has two curves and there are two P_f vs. σ_w plots for each test temperature.

5.5.1 Load VS. ΔD Plots

The Load VS. Diametrical Contraction plots are shoen below for different specimens at -50 Deg., -100 Deg., -150 Deg.

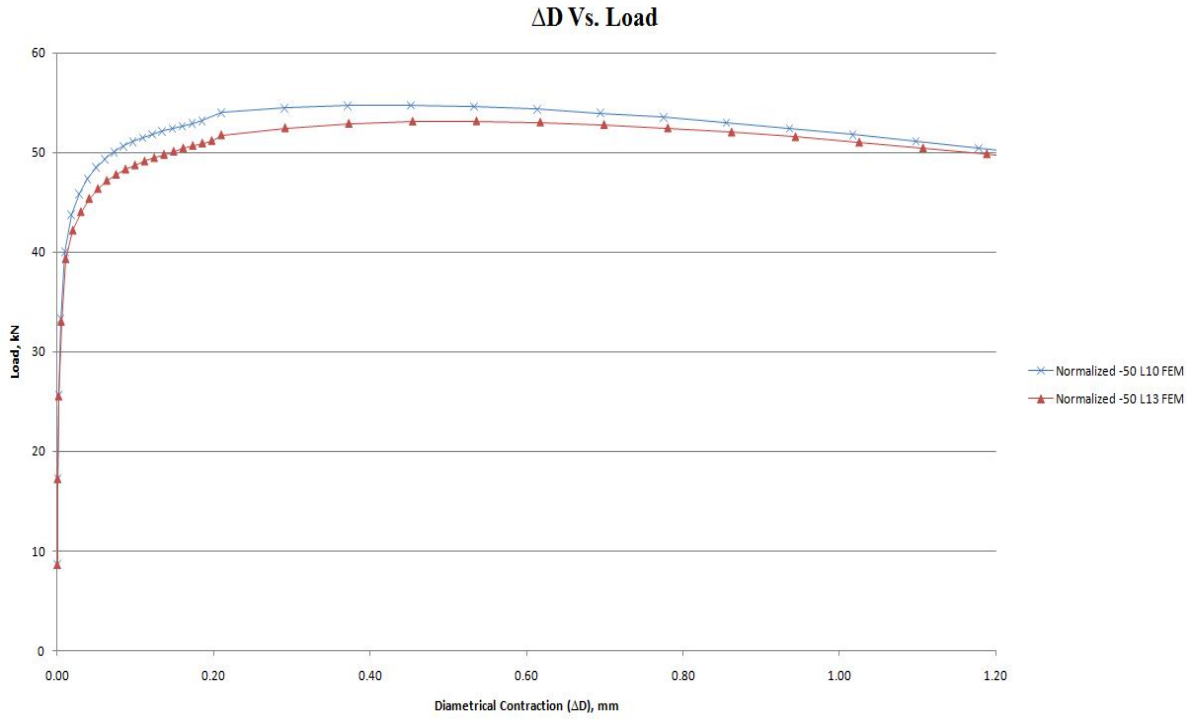

Figure 5 - 9 Normalized Load vs. ΔD plot for -50^{0}C

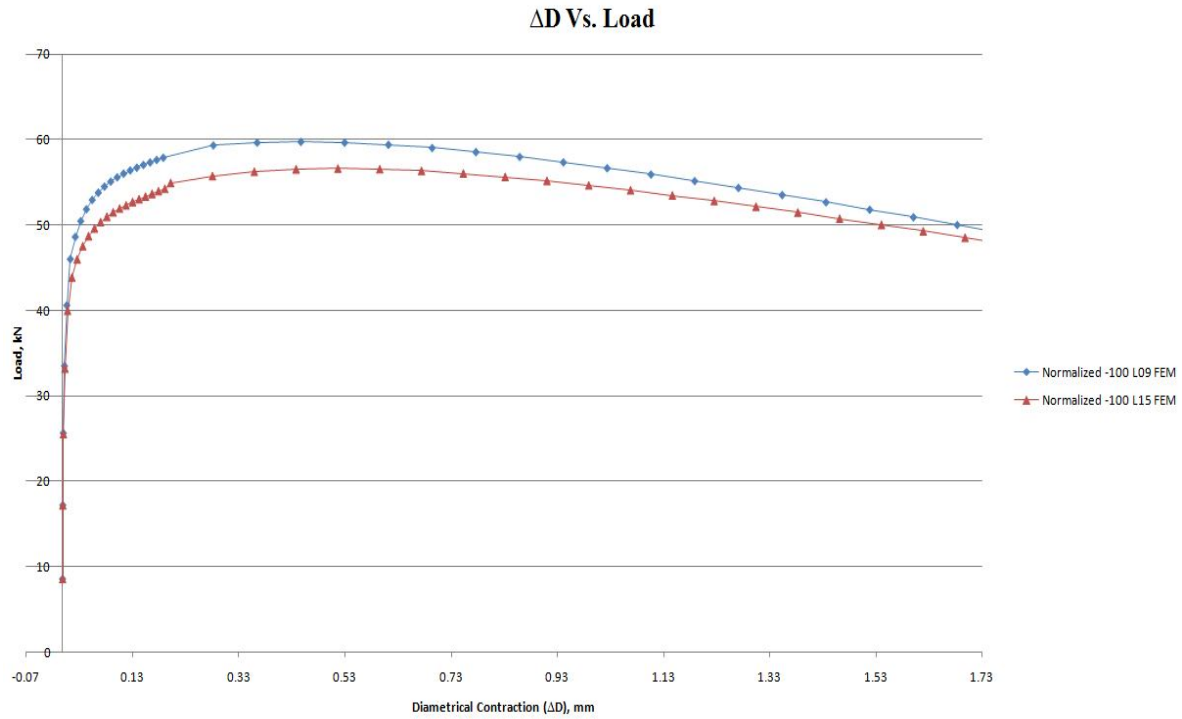

Figure 5 - 10 Normalized Load vs. ΔD plot for -100^{0}C

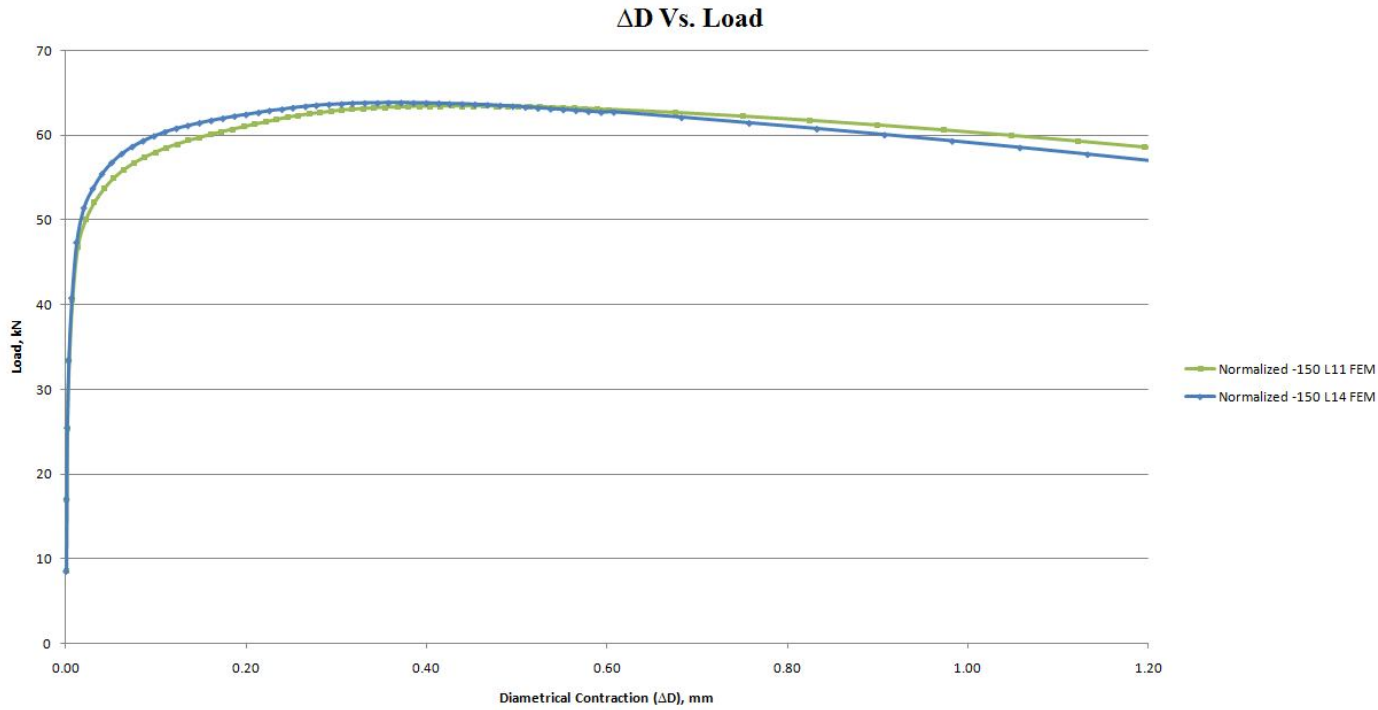

Figure 5 - 11 Normalized Load vs. ΔD plot for -50^{0}C.

The Load vs. ΔD data and maximum Load occurred during FE Analysis and corresponding ΔD values were obtained using Post Processor **LDPLOT** Its Apparent from Load vs. ΔD plots that after certain amount of diametrical contraction the load starts decreasing which is and also for different specimen tested at same temperature there is some variation in curves from each other that is because of variation in microstructure of specimens.

5.5.2 σ_u And 'm' For Various Temperatures

The Weibull Parameters for various temperatures are calculated are given below in table 5.1

S. No.	Test Temperature, ^{0}C	Specimen No.	σ_u	m
3	-50	L10	1223.868	51.282
4	-50	L13	1298.648	36.780
5	-100	L09	1912.807	19.285
6	-100	L15	1682.624	24.989
7	-150	L11	2267.170	26.908
8	-150	L14	2226.769	29.208

Table 5.1 Values of Beremin's parameters at different test temperatures

5.53 P_f VS. σ_w PLOTS FOR VARIOUS TEMPERATURES

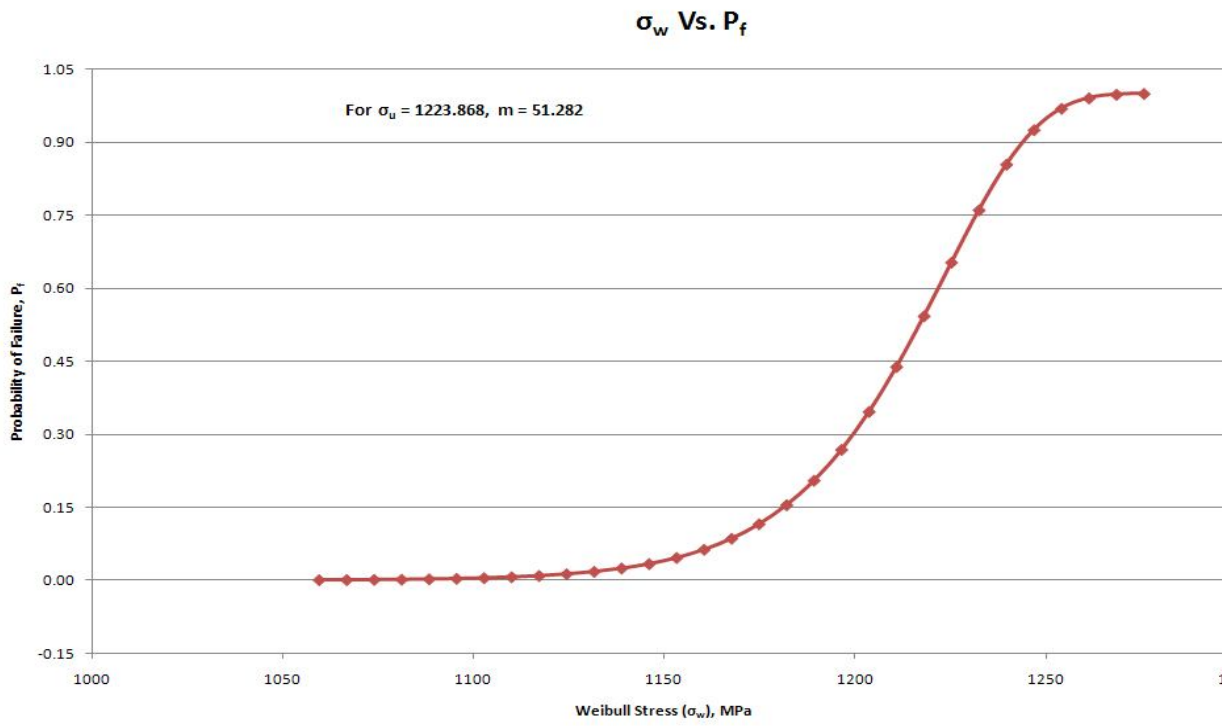

Figure 5 - 12 Pf vs. σw plot for sample L10 at -50 0C

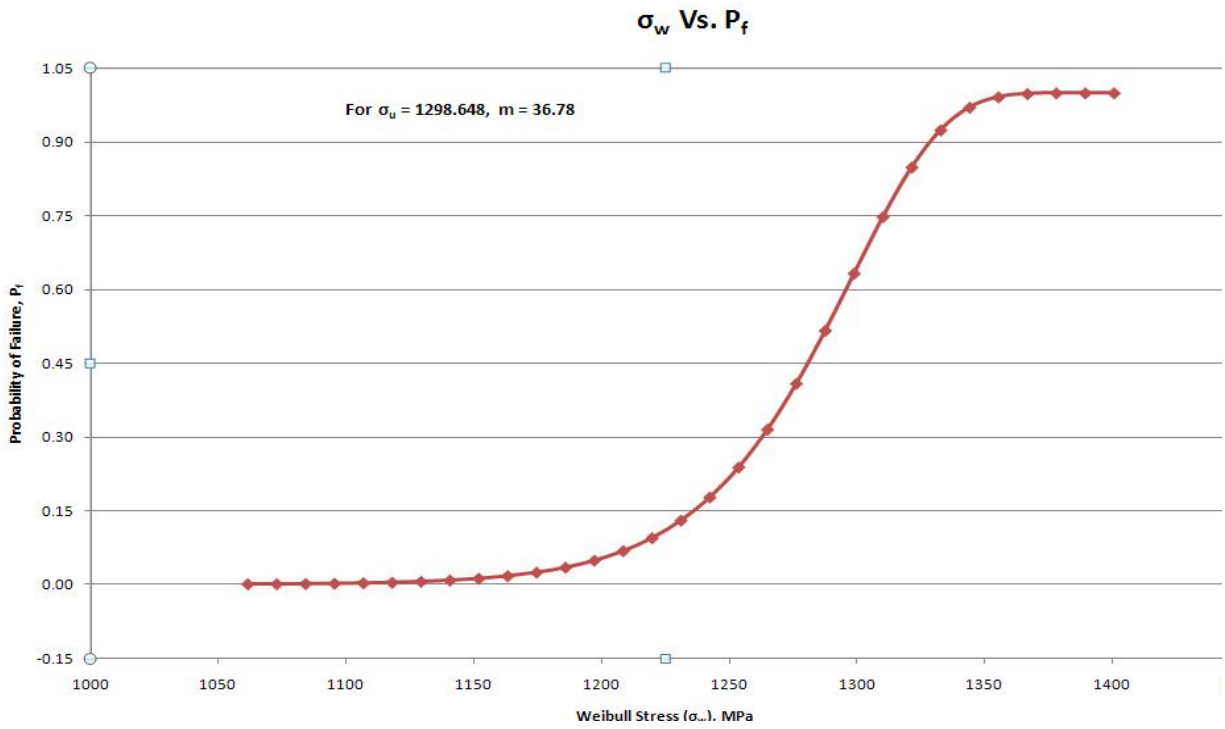

Figure 5 - 13 P_f vs. σ_w plot for sample L13 at -50 ^{0}C

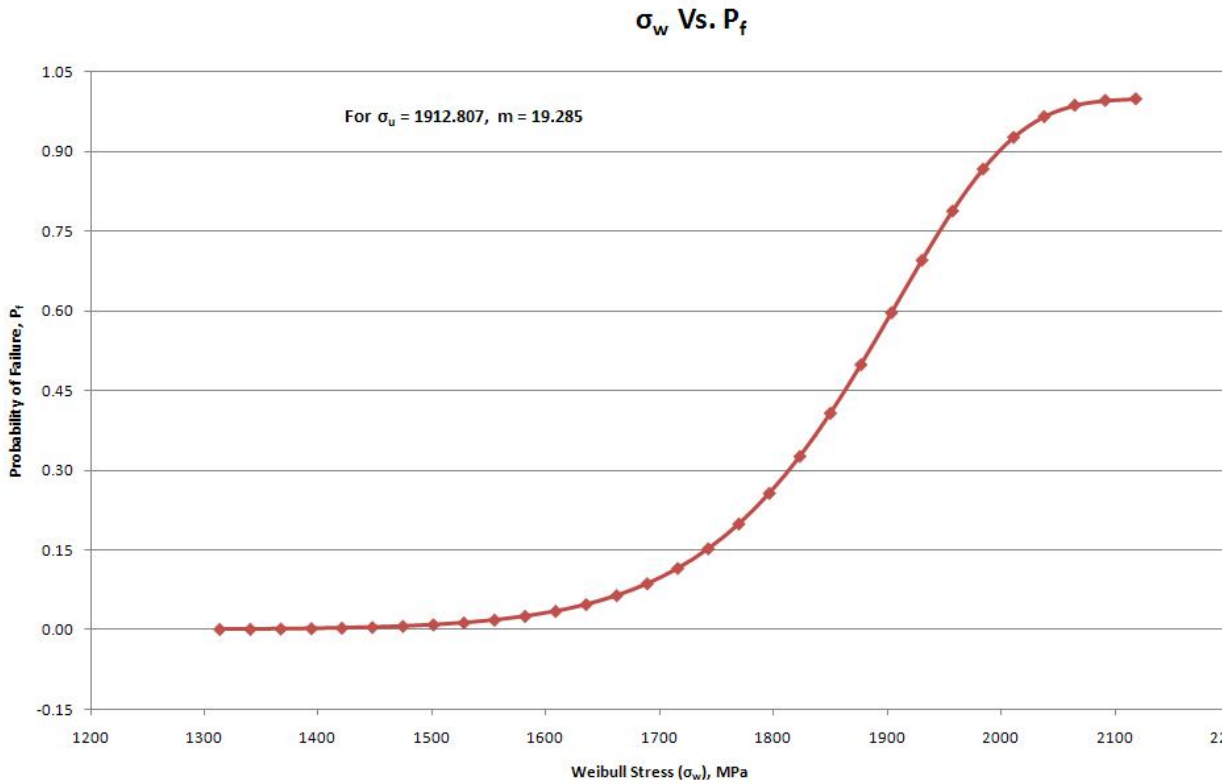

Figure 5 - 14 P_f vs. σ_w plot for sample L09 at -100 ^{0}C

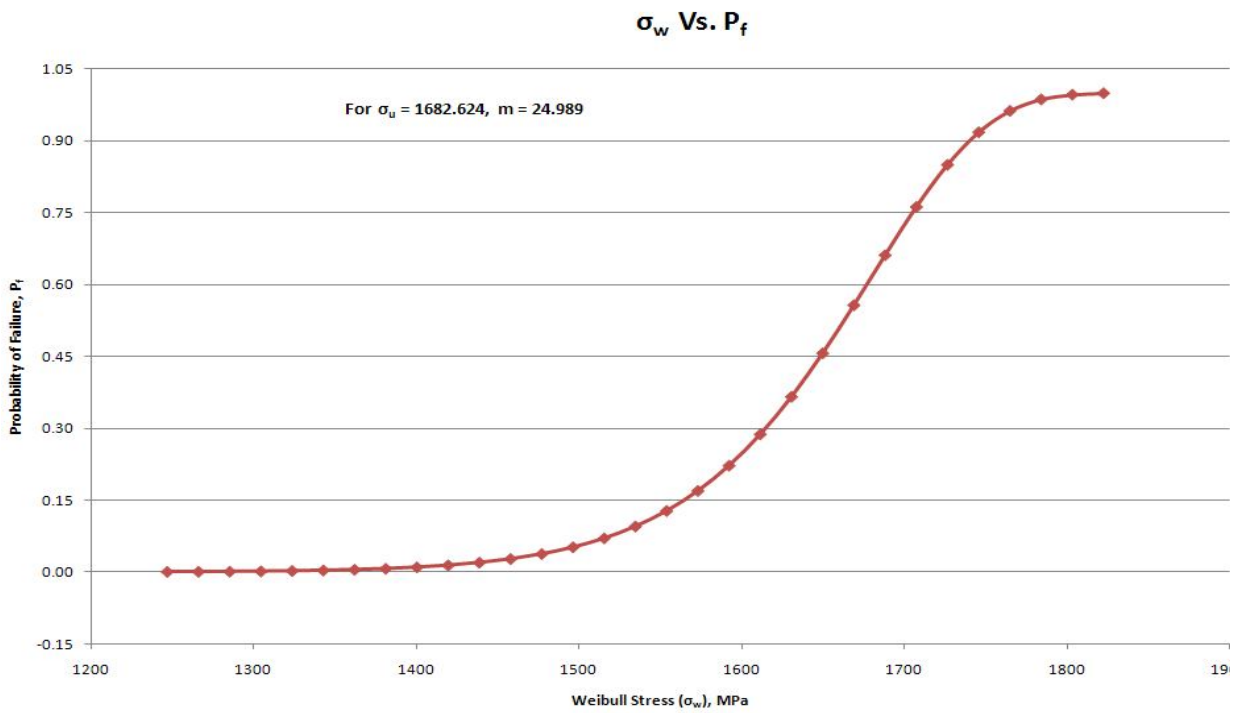

Figure 5 - 15 P_f vs. σ_w plot for sample L15 at -100 ^{0}C

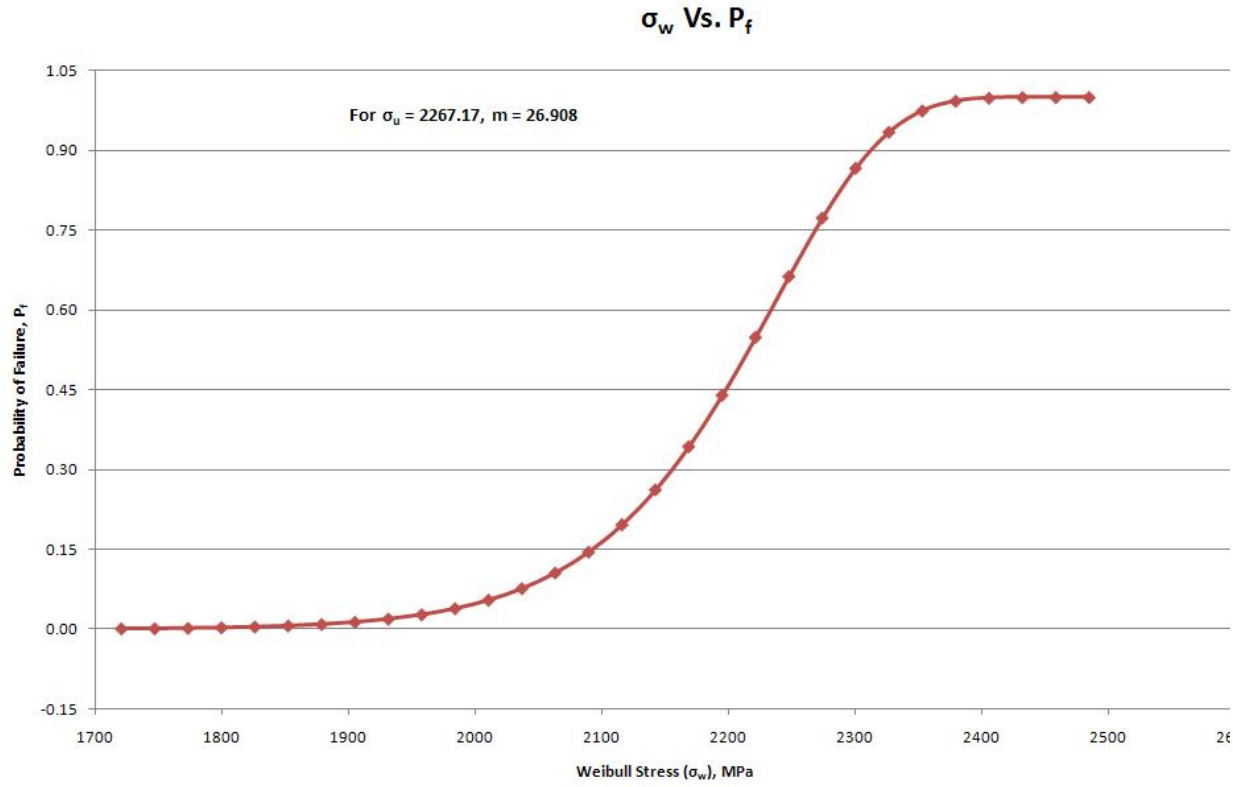

Figure 5 - 16 P_f vs. σ_w plot for sample L11 at -150 ^{0}C

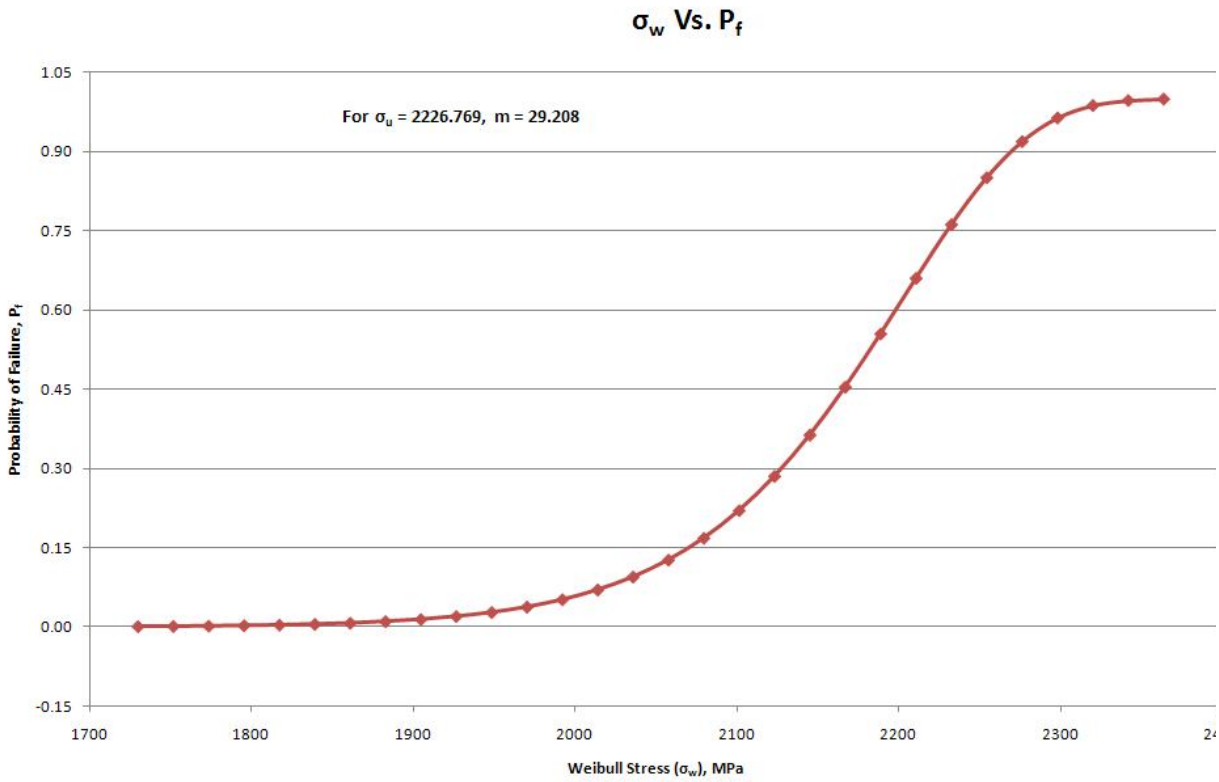

Figure 5 - 17 P_f vs. σ_w plot for sample L154 at -150 ^{0}C

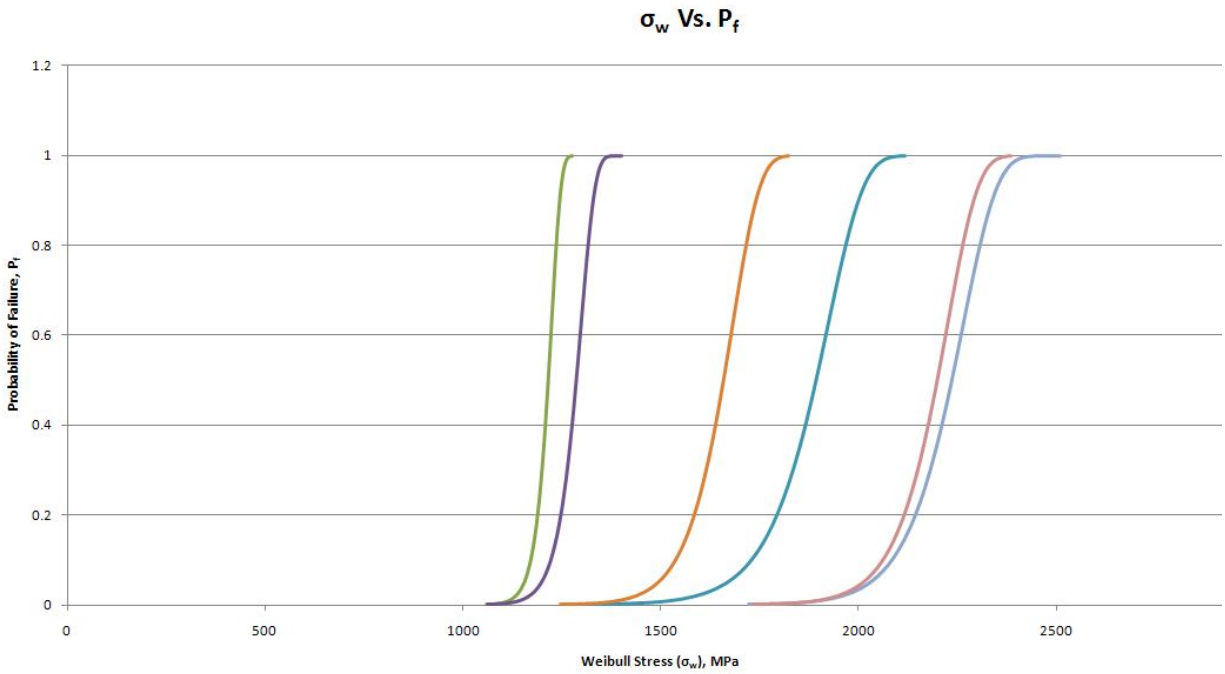

Figure 5 - 18 P_f vs. σ_w plot for all samples at -50 ^{0}C , -100 ^{0}C, -150 ^{0}C

CHAPTER 6

CLOUSRE

6.1 Conclusions

Cleavage fracture in alloy steel usually occurs by unstable micro-cracks initiated at brittle second phase inclusions. Because of large variation in parameters such as size, orientation and shape of these inclusions and the non-uniform stress field around a loaded crack-tip, the event of cleavage fracture follows a statistical nature. To predict the initiation of such fracture, Beremin's model of cleavage fracture based on weakest link theory has been used using two parameter Weibull statistics.. the procedure adopted during the present work is as follows.

1. A large number of grooved tensile specimens have been fabricated as per standards.
2. The specimens have been tested at 50 ^{0}C , -100 ^{0}C and -150 ^{0}C. Thirty specimens in each set.
3. The data collected during tests are 1.) specimen temperature and 2.) Load-displacement data.
4. Elastic Plastic analysis of test specimen have been performed and Load vs. diametrical contraction data was obtained.
5. Statistical analysis, based on "maximum likelyhood method" has been done to determine Beremin's parameters

It is apparent from the results that Beremin's parameters vary with temperature. The scaling Parameter 'σ_u' decreases with temperature. But '**m'** doesn't vary monotonically It has also been found that there is considerable effect of stress strain curve and yield strength on the Beremin's parameters as is clear from the variation in values of Beremin's parameters for same temperature. The possible explanation is the value of yield strength decides no. of elements having plastic deformation, thus different yield strength values gives different values of Beremin's temperature.

6.2 Scope for Future Work

To study the effect of specimen geometry on Beremin's Parameters different sets of identical Specimen should be tested at same temperatures.

To make a relationship between temperature and ‘m’ more experimentation should be done.

Also Experimentation on other materials should be done do compare the material behavior under cleavage fracture, which is of much importance in Nuclear Reactors Safe operation.

References

[1] **Landes, J.D., Shaffer, D.H.,** Fracture Mechanics, Twelfth Conference, ASTM STP 700, pp.368-382, Philadelphia, 1980

[2] **Beremin, F.M.,** Metallurgical Transactions A, Vol. 14A, 1983, pp. 2277-2287

[3] **Griffith, A.A.,** "The Phenomena of Rupture and Flow In Solids", Philosophical Transactions, Series A, Vol. 221, 1920, pp163-198

[4] **Irwin, G.R.,** "Fracture Dynamics", Fracturing of Metals, American society of metals, Cleveland, 1948,p 147-166

[5] **B. K. Dutta, et al.** "Temperature Dependency of Beremin's Parameters for 20MnMoNi55 Material", BARC Mumbai

[6] **Cleizergues et al** – "Development and Use of Beremin Local Criterion for Cleavage Fracture in the Steel Industry", Journal de Physique III, Volume 6, October 1996

[7] **Gy. B. Lenkey, et al –** "The Application of the Beremin Model for Predicting the Brittle Fracture Resistance " NATO Science Series II: Mathematics, Physics and Chemistry - Vol.78

[8] **A Mirzaee-Sisan, et al** – "Application of the Local Approach to Predict Brittle Fracture Following Local Compression", Department of Mechanical Engineering, University of Bristol, Queen's Building, University Walk, BS8 1TR, UK

[9] **D. Moinereau, et al.** - "Local Approach to Fracture Applied to Reactor Pressure Vessel: Synthesis of A Cooperative Programme Between EDF, CEA, Framatome and AEA", Journal de Physique III, Volume 6, October 1996

[10] **Gy. B. Lenkey, et al.** – "Application of The Beremin-Model for Predicting the Brittle Fracture Resistance of Steel for Spent Nuclear Fuel Containers", The 14th Bienniel Conference on Fracture (ECF 14), vol.II

[11] **Takashi Miyata, et al.** – "Mezzo-Scopic Analysis of Fracture Toughness in Steels", Mat. Res. vol.5 no.2 São Carlos June 2002

[12] **C. Ruggieri** –"A Micromechanics Approach to Quantify Strength Mismatch Effects on Fracture Behavior of Interface Cracks", Dept. of Naval Architecture and Ocean Engineering, University of São Paulo, SP 05508-900, Brazil

[13] **John, Vernon.** Introduction to Engineering Materials, 3rd ed., New York: Industrial Press, 1992. ISBN 0831130431

[14] **J.S. Lee, I.S. Kim, C.H. Jang and A. Kimura,** "Irradiation Embrittlement of Cladding and HAZ of RPV Steel"

[15] **MIT-Department of Nuclear Engineering** "LWR Pressure Vessel Embrittlement and Conditions of Validity of Current Predictive Methodologies"

[16] **O. P. Maksimkin, F. A. Garner, et al.** "Phase Transformations Observed In EP-450 Ferritic/Martensitic Steel Irradiated at 30 0c to 40.3 Dpa in the Bn-350 Fast Reactor" Institute of Nuclear Physics, National Nuclear Centre, Alma Ata, Kazakhstan and Pacific Northwest National Laboratory

[17] **D.R. Harries**, "Ferritic Martensitic Steels for Use in Near Term And Commercial Fusion Reactors", Proceedings of the Topical Conference on Ferritic Alloys for Use in Nuclear Energy Technologies, Snowbird, Utah, June 19-23, 1983.

Appendix 1

Maximum Likelihood method for determination of shape parameter 'm' and scaling parameter 'σ_u' (Weibull stress corresponding to 63.2% probability of failure)

In this approach, the values of two parameter 'm' and 'σ_u' are sought which result in a Weibull function which describes the experimental data which are most likely. The probability that, for an estimated set of Weibull parameters, the experimental results would have occurred should be maximised. This is equal to the probability that all 'σ_n' values occur simultaneously which is given by the product of all fracture probabilities:

$f_N = f(\sigma_1).f(\sigma_2).f(\sigma_3).....f(\sigma_n).....f(\sigma_{N-1}).f(\sigma_N)$. This is defined as the maximum likelihood function F_L which is given by:

$$F_L = \prod_{i=1}^{N} f(\sigma_{w_i}) \qquad \textbf{A1 - 1}$$

This function is to be maximised. To maximise the likelihood function 'F_L', the partial derivatives w.r.t. m and σ_u are set equal to zero. Since taking the derivatives of a sum is easier than that of their product, the derivation is done on the logarithm of F_L.

$$F_L = \prod_{i=1}^{N} f(\sigma_{w_i}) = \left(\frac{m}{\sigma_u}\right)^N . \prod_{i=1}^{N} \left(\frac{\sigma_{w_i}}{e_u}\right)^{m-1} . \exp\left\{-\sum_{i=1}^{N}\left(\frac{\sigma_{w_i}}{\sigma_u}\right)^m\right\} \qquad \textbf{A1 - 2}$$

$$\Rightarrow \ln F_L = \ln\left(\frac{m}{\sigma_u}\right)^N + \ln\prod_{i=1}^{N}\left(\frac{\sigma_{w_i}}{\sigma_u}\right)^{m-1} + \ln.\exp\left\{-\sum_{i=1}^{N}\left(\frac{\sigma_{w_i}}{\sigma_u}\right)^m\right\} \qquad \textbf{A1 - 3}$$

$$= N.\ln\left(\frac{m}{\sigma_u}\right) + \sum_{i=1}^{N}\ln\left(\frac{\sigma_{w_i}}{\sigma_u}\right)^{m-1} - \sum_{i=1}^{N}\ln\left(\frac{\sigma_{w_i}}{\sigma_u}\right)^m \qquad \textbf{A1 - 4}$$

For deriving the expression of σ_u, differentiate the function with respect to σ_u and put it to zero. It is given as:

$$\frac{\partial(\ln F_L)}{\partial \sigma_u} = 0 \qquad \textbf{A1 - 5}$$

$$\Rightarrow N.\frac{\sigma_u}{m}.m.\left(-\frac{1}{\sigma_u^2}\right) + (m-1).\sum_{i=1}^{N}\frac{\sigma_u}{\sigma_{w_i}}.\frac{\sigma_{w_i}}{(-\sigma_u^2)} - \sum_{i=1}^{N} m.\left(\frac{\sigma_{w_i}}{\sigma_u}\right)^{m-1}.\left(\frac{\sigma_{w_i}}{-\sigma_u^2}\right) = 0 \qquad \textbf{A1 - 6}$$

$$\Rightarrow -\frac{N}{\sigma_u} - (m-1).\frac{N}{\sigma_u} + m.\sum_{i=1}^{N}.\left(\frac{\sigma_{w_i}}{\sigma_u}\right)^{m}.\frac{1}{\sigma_u} = 0 - \frac{m}{\sigma_u}\left[N - \frac{1}{\sigma_u^m}\sum_{i=1}^{N}(\sigma_{w_i})^m\right] = 0 \qquad \textbf{A1 - 7}$$

$$\Rightarrow \sum_{i=1}^{N}(\sigma_{w_i})^m = N \Rightarrow \sigma_u = \sqrt[m]{\frac{1}{N}\sum_{i=1}^{N}(\sigma_{w_i})^m} \qquad \textbf{A1 - 8}$$

Again for deriving the expression for ‘m’, differentiate the function with respect to ‘m’ and put the expression equal to zero. It is given as:

$$\frac{\partial(\ln F_L)}{\partial m} = 0 \qquad \textbf{A1 - 9}$$

$$\Rightarrow N.\frac{\sigma_u}{m}.\frac{1}{\sigma_u} + \sum_{i=1}^{N}\ln\left(\frac{\sigma_{w_i}}{\sigma_u}\right) - \sum_{i=1}^{N}\left(\frac{\sigma_{w_i}}{\sigma_u}\right)^{m}.\ln\left(\frac{\sigma_{w_i}}{\sigma_u}\right) = 0 \qquad \textbf{A1 - 10}$$

$$\Rightarrow \frac{N}{m} + \sum_{i=1}^{N}\ln(\sigma_{w_i}) - \sum_{i=1}^{N}\ln\sigma_u - \left[\frac{\sum_{i=1}^{N}(\sigma_{w_i})^m.\ln(\sigma_{w_i})}{(\sigma_u)^m} - \frac{\sum_{i=1}^{N}(\sigma_{w_i})^m.\ln\sigma_u}{(\sigma_u)^m}\right] = 0 \qquad \textbf{A1 - 11}$$

Putting the expression for σ_u from Equation A2-1 in the above equation, we get:

$$\frac{N}{m} + \sum_{i=1}^{N}\ln(\sigma_{w_i}) - N.\ln\sigma_u - N.\frac{\sum_{i=1}^{N}(\sigma_{w_i})^m.\ln(\sigma_{w_1})}{\sum_{i=1}^{N}(\sigma_{w_i})^m} + \ln\sigma_u.\frac{\sum_{i=1}^{N}(\sigma_{w_i})^m}{\sum_{i=1}^{N}(\sigma_{w_i})^m}.N = 0 \qquad \textbf{A1 - 12}$$

$$\Rightarrow \frac{N}{m} + \sum_{i=1}^{N} \ln(\sigma_{w_i}) - N.\frac{\sum_{i=1}^{N}(\sigma_{w_i})^{m}.\ln(\sigma_{w_1})}{\sum_{i=1}^{N}(\sigma_{w_i})^{m}} = 0 \qquad \textbf{A1 - 13}$$

Equations A1-1 and A1-2 gives the expressions for determining σ_u and m respectively. Equation A1-2 has to be solved by an iterative process. Assume some initial value of 'm' and solve for the new value of 'm' till the two solutions converge each other.